

A supersonic turbulence origin of Larson’s laws

Alexei G. Kritsuk,^{1*} Christoph T. Lee¹ and Michael L. Norman^{1,2}

¹*Physics Department and CASS, University of California, San Diego, 9500 Gilman Drive, La Jolla, CA 92093-0424, USA*

²*San Diego Supercomputer Center, University of California, San Diego, 10100 Hopkins Drive, La Jolla, CA 92093-0505, USA*

Accepted 2013 September 23. Received 2013 September 23; in original form 2013 January 9

ABSTRACT

We revisit the origin of Larson’s scaling laws describing the structure and kinematics of molecular clouds. Our analysis is based on recent observational measurements and data from a suite of six simulations of the interstellar medium, including effects of self-gravity, turbulence, magnetic field and multiphase thermodynamics. Simulations of isothermal supersonic turbulence reproduce observed slopes in linewidth–size and mass–size relations. Whether or not self-gravity is included, the linewidth–size relation remains the same. The mass–size relation, instead, substantially flattens below the sonic scale, as prestellar cores start to form. Our multiphase models with magnetic field and domain size 200 pc reproduce both scaling and normalization of the first Larson law. The simulations support a turbulent interpretation of Larson’s relations. This interpretation implies that: (i) the slopes of linewidth–size and mass–size correlations are determined by the inertial cascade; (ii) none of the three Larson laws is fundamental; (iii) instead, if one is known, the other two follow from scale invariance of the kinetic energy transfer rate. It *does not* imply that gravity is dynamically unimportant. The self-similarity of structure established by the turbulence breaks in star-forming clouds due to the development of gravitational instability in the vicinity of the sonic scale. The instability leads to the formation of prestellar cores with the characteristic mass set by the sonic scale. The high-end slope of the core mass function predicted by the scaling relations is consistent with the Salpeter power-law index.

Key words: turbulence – methods: numerical – stars: formation – ISM: structure.

1 INTRODUCTION

Understanding physics underlying structure formation and evolution of molecular clouds (MCs) is an important stepping stone to a predictive statistical theory of star formation (McKee & Ostriker 2007). Statistics of non-linear density, velocity, and magnetic field fluctuations in MCs may have imprints in the star formation rate and the stellar initial mass function (Krumholz & McKee 2005; Hennebelle & Chabrier 2011; Padoan & Nordlund 2011, 2002; Padoan et al. 2007; Hennebelle & Chabrier 2008). Non-linear coupling of self-gravity, turbulence and magnetic field in MCs is believed to regulate star formation (Mac Low & Klessen 2004). But how does this actually work? Answering this question would ultimately help one to break new ground for ab initio star formation simulations. This paper mostly deals with one particular aspect of the cloud structure formation, namely the interaction of turbulence and gravity, by confronting observations with numerical simulations and theory.

Larson (1981) established that for many MCs their internal velocity dispersion, σ_u , is well correlated with the cloud size, L , and mass, m . Since the power-law form of the correlation, $\sigma_u \propto L^{0.38}$, and the power index, $0.38 \sim 1/3$, were similar to those of the Kolmogorov (1941a,b, hereafter K41) turbulence, he suggested that observed non-thermal linewidths may originate from a ‘common hierarchy of interstellar turbulent motions’. The clouds would also *appear* mostly gravitationally bound and in approximate virial equilibrium, as there was a close positive correlation between their velocity dispersion and mass, $\sigma_u \propto m^{0.20}$. However, Larson suggested that these structures ‘cannot have formed by simple gravitational collapse’ and should be at least partly created by supersonic turbulence. This seminal paper preconceived many important ideas in the field and strongly influenced its development for the past 30 years.

Myers (1983) studied 43 smaller dark clouds and confirmed the existence of significant linewidth–size and density–size correlations found earlier by Larson for larger MCs. He acknowledged that two distinct interpretations of the data are possible: (i) the linewidth-size relation also known as Larson’s first law ($\sigma_u \propto R^{0.5}$) arises from a Kolmogorov-like cascade of turbulent energy; (ii) the same

* E-mail: akritsuk@ucsd.edu

relation results from the tendency of clouds to reside in virial equilibrium ($\sigma_u \propto \rho^{0.5}R$, Larson’s second law) and from the tendency of the mean cloud density to scale inversely linearly with the cloud size ($\rho \propto R^{-1}$, Larson’s third law). He concluded that the available data ‘do not permit a clear choice between these interpretations’.

Solomon et al. (1987, hereafter SRBY87) confirmed Larson’s study using observations of ^{12}CO emission with improved sensitivity for a more homogeneous sample of 273 nearby clouds. Their linewidth–size relation, $\sigma_u = 1.0 \pm 0.1S^{0.5 \pm 0.05} \text{ km s}^{-1}$, however, had a substantially steeper slope than Larson’s, more reminiscent of that for clouds in virial equilibrium,¹

$$\sigma_u = (\pi G \Sigma)^{1/2} R^{1/2}, \quad (1)$$

partly because the SRBY87 clouds had approximately constant molecular gas surface density ($\Sigma \propto \rho R \approx \text{const.}$) independent of their size. The surface density–size relation – another form of Larson’s third law – can be derived by eliminating σ_u from his first two relations: $\Sigma \propto mL^{-2} \propto L^{0.38/0.20-2} \propto L^{-0.1}$. Thus any two of Larson’s laws imply the other, leaving open a question of which two laws, if any, are actually fundamental.

Whether or not the third law simply reflects observational selection effects stemming from limitations in dynamic range of available observations is still a matter of debate (Larson 1981; Kegel 1989; Scalo 1990; Ballesteros-Paredes & Mac Low 2002; Schneider & Brooks 2004). Lombardi, Alves & Lada (2010) studied the structure of nearby MCs by mapping the dust column density that is believed to be a robust tracer for the molecular hydrogen (cf. Padoan et al. 2006). The dust extinction maps usually have a larger (although not much larger) dynamic range (typically $\gtrsim 10^2$) than that feasible with simple molecular tracers. Lombardi et al. (2010) verified Larson’s third law ($\Sigma \approx \text{const.}$) with a very small scatter for their MCs defined with a given extinction threshold. This trivial result is determined by how the size of a cloud or clump is defined observationally and is physically insignificant (see also Ballesteros-Paredes, D’Alessio & Hartmann 2012). Lombardi et al. (2010) also demonstrated that the mass–size version ($m \propto R^2$) of the third law applied within a single cloud using different thresholds does not hold, indicating that individual clouds cannot be described as objects characterized by constant column density. Three-dimensional numerical simulations that are free of such selection effects nevertheless reproduce a robust mass–size correlation for density structures in supersonic turbulence with a slope of 2.3 – 2.4, i.e. steeper than $m \propto R^2$ (Ostriker, Stone & Gammie 2001; Kritsuk et al. 2007a, 2009). Thus simulations do not support the constant aver-

age column density hypothesis and qualitatively agree with single-cloud results of Lombardi et al. (2010).

Assuming that $\Sigma = \text{const.}$ for all clouds, SRBY87 evaluated the ‘X-factor’ to convert the luminosity in ^{12}CO (1–0) line to the MC mass. It would seem that the new power index value ~ 0.5 ruled out Larson’s hypothesis that the correlation reflects the Kolmogorov law. In the absence of robust predictions for the velocity scaling in supersonic turbulence (cf. Passot et al. 1988), a simple virial equilibrium-based interpretation of linewidth–size relation appealed to many in the 1980s. The central supporting observational evidence for a gravitational origin of Larson’s relations has been the scaling coefficient in the first law, which coincided with the predicted value for gravitationally bound clouds $\sim \sqrt{\pi G \Sigma}$. In particular, the observed gravitational energy of giant molecular clouds (GMCs) in the outer Galaxy with the total molecular mass in excess of $\sim 10^4 M_\odot$ was found comparable to their observed kinetic energy (Heyer, Carpenter & Snell 2001).

Since then views on this subject have remained polarized. For instance, Ballesteros-Paredes et al. (2011a,b) argue that MCs are in a state of ‘hierarchical and chaotic gravitational collapse’, while Dobbs, Burkert & Pringle (2011) believe that GMCs are ‘predominantly gravitationally unbound objects’. As some authors tend to deny the existence of a unique linewidth–size relation outright, acknowledging the possibility that different clouds may exhibit different trends (e.g. Ballesteros-Paredes et al. 2011a), others argue that it is difficult to identify the relation using samples that have too small a dynamic range. In addition, the scaling laws based on observations of different tracers may differ as they probe different density regimes and different physical structures (Hennebelle & Falgarone 2012).

This persistent dualism in interpretation largely stems from the fundamentally limited nature of information that can be extracted from observations (e.g. due to low resolution, projection effects, wide variation in the CO–H₂ conversion factor, active feedback in regions of massive star formation, etc.) (Shetty et al. 2010) and from our limited understanding of supersonic turbulence (e.g. Ballesteros-Paredes et al. 2007). Early on, supersonic motions were thought to be too dissipative to sustain a Kolmogorov-like cascade. Later, numerical simulations showed that direct dissipation in shocks constitutes a small fraction of total dissipation and that turbulent velocities have the Kolmogorov scaling (Passot, Pouquet & Woodward 1988; Porter, Pouquet & Woodward 1994; Falgarone et al. 1994). This result based on simulations at Mach numbers around unity left the important role of strong density fluctuations underexposed (cf. Fleck 1983, 1996) up until simulations at higher Mach numbers demonstrated that the velocity scaling is in fact non-universal (Kritsuk et al. 2006a).

The key point of contention is the question of whether the hierarchically structured clouds represent quasi-static bound objects in virial *equilibrium* over approximately four decades in linear scale (e.g. SRBY87; Chieze 1987) or instead they represent *non-equilibrium* dissipative structures borne in the self-gravitating turbulent interstellar medium (ISM; e.g. Fleck 1983; Elmegreen & Scalo 2004; Mac Low & Klessen 2004; Lequeux 2005; Ballesteros-Paredes et al. 2007;

¹ We deliberately keep the original notation used by different authors for the cloud size (e.g. the size parameter in parsecs, $S = D \tan(\sqrt{\sigma_l \sigma_b})$; the maximum projected linear extent, L ; the radius, $R = \sqrt{A/\pi}$, defined for a circle with area, A , equivalent to that of cloud) to emphasize ambiguity and large systematic errors in the cloud size and mass estimates due to possible line-of-sight confusion, ad hoc cloud boundary definitions (Heyer et al. 2009), and various X-factors involved in conversion of a tracer surface brightness into the H₂ column density.

Hennebelle & Falgarone 2012). While both original interpretations of Larson's laws adopt the same form of the Navier–Stokes (N-S) equation as the starting point of their analyses, distinct conclusions for the origin of the observed correlations are ultimately drawn.

Note that the two interpretations are mutually exclusive in the presence of large-scale turbulence with the energy injection length-scale of the order of the Galactic molecular disc thickness. This description of the ISM turbulence is supported by the extent of the observed linewidth–size and mass–size correlations which continue up to ~ 100 pc with no sign of flattening (Hennebelle & Falgarone 2012) as well as by simulations of supernova-driven ISM turbulence, which suggest the integral scale of 75 – 100 pc (Joung & Mac Low 2006; de Avillez & Breitschwerdt 2007; Gent et al. 2013). There have been scenarios, where self-gravitating clouds are instead microturbulent (e.g. White 1977). For such clouds and their substructure, virial analysis would be rigorously justified down to the integral scale of microturbulence (Chandrasekhar 1951; Bonazzola et al. 1987, 1992; Schmidt & Federrath 2011). If turbulence were driven within clouds by their own collapse, virial analysis would be applicable to the whole clouds only. In this case, however, turbulent velocities would originate from and get amplified by gravitational collapse of the cloud (e.g. Henriksen & Turner 1984; Zinnecker 1984; Biglari & Diamond 1988; Henriksen 1991). Hence one would naively expect $\sigma_u \propto R^{-1/2}$, which contradicts the observed linewidth–size relation (Robertson & Goldreich 2012).

In essence, the discrepancy between turbulent and virial interpretations can be tracked back to the ansatz, used to derive the virial theorem from the N-S equation in the form of the Lagrange identity,

$$2(E_{\text{kin}} + E_{\text{int}}) + E_{\text{mag}} - E_{\text{grav}} = 0, \quad (2)$$

routinely applied to MCs (e.g. McKee & Zweibel 1992; Ballesteros-Paredes 2006). This form is incompatible with the basic nature of the direct inertial cascade as it ignores the momentum density flux across the fixed Eulerian cloud boundary that is generally of the same order as the volume terms (e.g. Dib et al. 2007). Numerical simulations show that in star-forming clouds large turbulent pressure does not provide mean support against gravity. Instead, turbulent support in self-gravitating media is on average negative, i.e. promoting the collapse rather than resisting it (Klessen 2000; Schmidt, et al. 2013). Thus neither virial balance condition (1) nor energy equipartition condition $E_{\text{kin}}(R) \sim E_{\text{grav}}(R)$ can actually guarantee boundedness of clouds embedded in the general field of large-scale turbulence. Since virial conditions (1) and (2) do not comply with the N-S equation in the presence of large-scale turbulence, the fact that some of the most massive GMCs follow the first Larson law with a coefficient $\sim \sqrt{\pi G \Sigma}$ can be merely coincidental. This does not rule out a role for gravity in MC dynamics, as otherwise the clouds would never form stars or stellar clusters.

Recent progress in observations, theory and numerical simulations of ISM turbulence prompts us to revisit the origin of Larson's relations. In Section 2, we describe the simulations that will be used in Section 3 to give a computational perspective on the origin of the first Larson law. Section 4 continues the discussion with the mass–size relation. In Sec-

tion 5, we briefly introduce the concept of supersonic turbulent energy cascade and, using dimensional arguments, show that scaling exponents in the linewidth–size and mass–size relations are algebraically coupled. We then derive a secondary relation between column density and size in several different ways and demonstrate consistency with observations, numerical models and theory. We argue that the turbulent interpretation of Larson's laws implies that *none of the three laws is fundamental*, but that if one is known the other two follow directly from the scale invariance of the turbulent energy density transfer rate. Section 6 deals with the effects of self-gravity on small scales in star-forming clouds, and discusses the origin of the observed mass–size relation and the mass function for prestellar cores. Finally, in Section 7 we formulate our conclusions and emphasize the statistical nature of the observed scaling laws.

2 SIMULATIONS

In our analysis, we rely on data from a suite of six ISM simulations that include the effects of self-gravity, turbulence, magnetic fields and multiphase thermodynamics. The simulations use cubic computational domains with periodic boundary conditions. All models use large-scale forcing (Mac Low 1999) to mimic the energy flux incoming from scales larger than the box size. In all cases, the power in the driving acceleration field is distributed approximately isotropically and uniformly in the wavenumber interval $k/k_{\text{min}} \in [1, 2]$, where $k_{\text{min}} = 2\pi/L$ and L is the domain size. For convenience, we further divide the models in two classes, hydrodynamic (HD) and magnetohydrodynamic (MD); Table 1 summarizes model parameters and physics included in the simulations.

The set of three HD simulations were run with the ENZO code² (The Enzo Collaboration 2013), which uses the third order accurate piecewise parabolic method (PPM; Colella & Woodward 1984). The MD simulations employed an MHD extension of the method developed by Ustyugov et al. (2009). Model HD1 and all MD models used purely solenoidal driving, while models HD2 and HD3 were driven with a mixture of solenoidal and compressive motions. The inertial range ratio of compressive-to-solenoidal motions, and its dependence on Mach number and magnetic fields, is discussed in Kritsuk et al. (2010). All HD models assume an isothermal equation of state (EOS). As models HD1 and HD2 do not include self-gravity, they only depend on the sonic Mach number, details of forcing aside. In addition, three dimensional parameters: (i) the box size, L ; (ii) the mean density, ρ_0 ; and (iii) the temperature, T (or sound speed, c_s), fully determine the physical model. Typical values corresponding to MC conditions: $L = 1 - 5$ pc, $\rho_0/(\mu m_{\text{H}}) = 10^{2-3} \text{ cm}^{-3}$, and $c_s = 0.2 \text{ cm s}^{-1}$ for $T = 10$ K. The rms Mach number was chosen to be approximately 6, which is a good choice for the adopted range of L . Models with substantially larger physical domain sizes cannot take advantage of a simple isothermal EOS.

The HD3 simulation with self-gravity was earlier presented in Padoan et al. (2005) and Kritsuk et al. (2011b).

² <http://enzo-project.org>

Table 1. Simulation parameters.

Model	L (pc) (1)	N_{root} (2)	AMR (3)	ρ_0/m_{H} (cm^{-3}) (4)	u_{rms} (km s^{-1}) (5)	G (6)	B_0 (μG) (7)	EOS (8)	χ_{comp} (9)	Section (10)	Figure (11)	Reference (12)
HD1	1	2048 ³	—	1	6	0	—	IT	0	3.1, 4	1, 5	Kritsuk et al. (2009)
HD2	1	1024 ³	—	1	6	0	—	IT	0.4	3.1, 4	6	Kritsuk et al. (2007a)
HD3	5	512 ³	5×4	10 ³	6	1	—	IT	0.4	3.2, 6	2, 8	Kritsuk et al. (2011b)
MD1	200	512 ³	—	5	16	0	0.95	MP	0	3.3	3, 4	Kritsuk et al. (2011a)
MD2	200	512 ³	—	5	16	0	3.02	MP	0	3.3	3, 4	Kritsuk et al. (2011a)
MD3	200	512 ³	—	5	16	0	9.54	MP	0	3.3	3, 4	Kritsuk et al. (2011a)

Notes. For each model, the following information is provided: (1) domain size in parsecs, dimensionless for scale-free models HD1 and HD2; (2) uniform (root) grid resolution; (3) AMR settings: number of levels \times refinement factor; (4) mean number density in cm^{-3} , dimensionless for the scale-free models HD1 and HD2; (5) rms velocity in km s^{-1} , replaced by the rms Mach number for isothermal models; (6) boolean gravity switch: 1 if included, 0 – otherwise; (7) the mean magnetic field strength; (8) equation of state: isothermal (IT) or multiphase (MP); (9) χ_{comp} is the ratio of dilatational-to-total power in the external large-scale acceleration driving the turbulence; (10) Sections, where the results of the particular simulation are presented and discussed; (11) Figures, where the data from the simulation are presented.

Model HD3 was initiated on a 512^3 grid with a uniform density and a random initial large-scale velocity field. The implementation of driving in the ENZO code followed Mac Low (1999), wherein small static velocity perturbations are added every time step such that kinetic energy input rate is constant. Once turbulence has had enough time to develop and statistically stationary conditions were reached, we switched gravity and adaptive mesh refinement (AMR) on and halted the driving. Note that the kinetic energy decay in the short duration of the collapse phase is insignificant. Five levels of AMR were used (with a refinement factor of 4) conditioned on the Jeans length following the Truelove et al. (1997) numerical stability criterion. The model thus covered a hierarchy of scales from 5 pc (the box size) down to 2 au with an effective grid resolution of $(5 \times 10^5)^3$.

The multiphase models MD1–3 represent a set of simple periodic box models, which ignore gas stratification and differential rotation in the disc and employ an artificial large-scale solenoidal force to mimic the kinetic energy injection from various galactic sources. This naturally leads to an upper bound on the box size, L , which determines our choice of $L = 200$ pc. The MD models are fully defined by the following three parameters (all three would ultimately depend on L): (i) the mean gas density in the box, n_0 ; (ii) the rms velocity, $u_{\text{rms},0}$; and (iii) the mean magnetic field strength, B_0 , see Table 1 for numeric values and grid resolutions. The models also assume a volumetric heating source due to the far-ultraviolet (FUV) background radiation. This FUV radiation from OB associations of quickly evolving massive stars that form in MCs is the main source of energy input for the neutral gas phases and this source is in turn balanced by radiative cooling (Wolfire et al. 1995). The MD models were initiated with a uniform gas distribution with an addition of small random isobaric density perturbations that triggers a phase transition in the thermally bi-stable gas that quickly turns $\sim 25 - 65$ per cent of the gas mass into the thermally stable cold phase (CNM with temperature below $T = 184$ K), while the rest of the mass is shared between the unstable and stable warm gas (WNM). The CNM and WNM each contain roughly ~ 50 per cent of the total HI mass in agreement with observations (Heiles & Crutcher 2005). We then turn on the forcing and after a few large-

eddy turnover times (~ 10 Myr) the simulations approach a statistical steady state. If we replace this two-stage initiation process with a one-stage procedure by turning the driving on at $t = 0$, the properties of the steady state remain unchanged. The rms magnetic field is amplified by the forcing and saturates when the relaxation in the system results in a steady state. The level of saturation depends on B_0 and on the rate of kinetic energy injection by the large-scale force, which is in turn determined by u_{rms} and n_0 . This level can be easily controlled with the model parameters. In the saturated regime, models MD2 and MD3 tend to establish the kinetic/magnetic energy equipartition while the saturation level of magnetic energy in model MD1 is a factor of ~ 3 lower than the equipartition level. The mean thermal energy also gets a slight boost due to the forcing, but remains subdominant in all three models. More detail on the MD models will follow in § 3.3.

3 THE LINEWIDTH–SIZE RELATION

Recently, new methods of statistical analysis have been developed that provide diagnostics less ambiguous than the original linewidth–size scaling based on the estimates of velocity dispersion and cloud size or on two-point statistics of the emission line centroid velocity fluctuations (Miesch & Bally 1994). One example is the multivariate statistical technique of principal component analysis (PCA; Heyer & Schloerb 1997), allowing one to extract the statistics of turbulent interstellar velocity fluctuations in a form that can be directly compared to the velocity statistics routinely obtained from numerical simulations. Using the PCA technique, Heyer & Brunt (2004) found that the scaling of velocity structure functions (SFs) of 27 GMCs is close to invariant,

$$S_1(u, \ell) \equiv \langle |\delta u_\ell| \rangle = u_0 \ell^{0.56 \pm 0.02}, \quad (3)$$

for structures of size $\ell \in [0.03, 50]$ pc (see also Brunt 2003a,b). Here $\delta u_\ell = u(r) - u(r + \ell)$ is the velocity difference between two points in a three-dimensional volume separated by a lag ℓ . Note that the lengths ℓ entering this relation are the characteristic scales of the PCA eigenmodes; therefore,

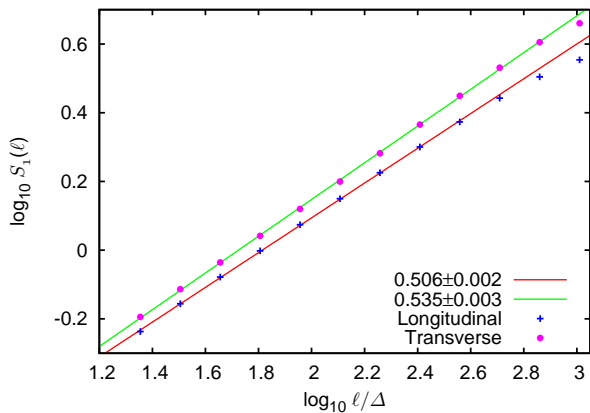


Figure 1. Scaling of the first-order transverse (green) and longitudinal (red) velocity SFs in model HD1 (compare with HD2, fig. 10 in Kritsuk et al. 2007a). Δ is the grid spacing. Numbers in the legend represent power-law indices for the linear least-squares representation of the data in the range $\log_{10}(\ell/\Delta) \in [1.2, 2.7]$ and formal uncertainty of the fits.

they may differ from the cloud sizes defined in other ways (e.g. McKee & Ostriker 2007). See also Roman-Duval et al. (2011) for a detailed discussion of the relation between the PCA-determined SFs and ‘standard’ first-order SFs obtained from simulations.

Heyer et al. (2009) later used observations of a lower opacity tracer, ^{13}CO , in 162 MCs with improved angular and spectral resolution to reveal weak systematic variations of the scaling coefficient, u_0 , in (3) with ℓ and Σ . Motivated by the concept of clouds in virial equilibrium, they introduced a new scaling coefficient $u'_0 \equiv \langle |\delta u_\ell| \rangle \ell^{-1/2} \propto \Sigma_\ell^{0.5}$. This correlation, if indeed observed with a high level of confidence, would indicate a departure from ‘universality’ for the velocity SF scaling (3) found earlier by Heyer & Brunt (2004) and compliance with the virial equilibrium condition (1) advocated by SRBY87.

Various scenarios employed in the interpretation of observations create a confusing picture of the structure formation in star-forming clouds carefully documented in a number of reviews (e.g. Blitz 1993; Elmegreen & Scalo 2004; Mac Low & Klessen 2004; Ballesteros-Paredes et al. 2007; McKee & Ostriker 2007; Hennebelle & Falgarone 2012). How can the apparent conspiracy between turbulence and gravity in MCs be understood and resolved? Analysis of data from numerical experiments will help us to shed some light on the nature of the confusion in three subsections that follow.

3.1 Isothermal models

Numerical simulations of isothermal supersonic turbulence without self-gravity render inertial range scaling exponents for the first-order velocity SFs that are similar to those measured by Heyer & Brunt (2004). Model HD2 gives $S_1(u, \ell) \propto \ell^{\zeta_1}$ with $\zeta_{1,\parallel} = 0.53 \pm 0.02$ and $\zeta_{1,\perp} = 0.55 \pm 0.04$ for longitudinal and transverse SFs, respectively. The rms sonic Mach number used in these simulations ($M_s = 6$) corresponds to MC size $\ell \approx 2$ pc, i.e. right in the middle of the observed scaling range. The simulation results indicate that velocity

scaling in supersonic regimes strongly deviates from Kolmogorov’s predictions for fluid turbulence. This removes one of the SRBY87 arguments against Larson’s hypothesis of a turbulent origin for the linewidth–size relation. Indeed, the scaling exponent of 0.50 ± 0.05 measured in SRBY87 for whole clouds and a more recent and accurate measurement 0.56 ± 0.02 by Heyer & Brunt (2004) that includes cloud substructure both fall right within the range of expected values for supersonic isothermal turbulence at relevant Mach numbers. Note, however, that the distinction between scaling ‘inside clouds’ and ‘between clouds’ often used in observational literature is specious if clouds are not isolated entities but rather part of a turbulence field (they are being constantly buffeted by their surroundings) on scales of interest even though they might look as isolated in projection (e.g. Henriksen & Turner 1984). Also note that the scaling exponent measured in SRBY87 is based on the velocity dispersion, i.e. it is more closely related to the exponent of the second-order SF of velocity, $\zeta_2/2$, and should be compared to $\zeta_{2,\parallel}/2 \approx 0.48$ and $\zeta_{2,\perp}/2 \approx 0.49$ obtained in model HD2.

Numerical simulations indicate that the power-law index ζ_1 is not universal, as it depends on the Mach number and also on the way the turbulence is forced. At higher Mach numbers, the slope is expected to be somewhat steeper, while a reduction of compressive component in the forcing would make it somewhat shallower. Schmidt et al. (2009) obtained $\zeta_{1,\perp} = 0.54 \pm 0.01$ for purely compressive forcing at $M_s \simeq 2.3$ in a simulation with grid resolution of 768^3 . If the force is solenoidal, velocity SFs tend to show slightly smaller exponents due to an effective reduction in compressive motions at large scales. Naturally, the effect is more pronounced in SFs of longitudinal velocities, which track compressive motions more closely. Fig. 1 illustrates this point with data from model HD1, where $\zeta_{1,\parallel} \simeq 0.51$ and $\zeta_{1,\perp} \simeq 0.54$.

The significance of the scaling dependence on the forcing found in numerical simulations should not be overestimated, though, due to their typically very limited dynamic range. It is not a priori clear whether the integral scale of the turbulence has to be the same in simulations with the same grid resolution that employ widely different forcing. In supersonic turbulence at very high Reynolds numbers, the solenoidal and dilatational modes are locally strongly coupled due to non-linear mode interactions in spectral space (Kritsuk et al. 2007a). This locks the dilatational-to-solenoidal ratio at the geometrically motivated natural level of $\sim 1/2$ (Nordlund & Padoan 2003), which appears to be a universal asymptotic limit supported by turbulence decay simulations (Kritsuk et al. 2010). Whether or not currently available models with compressive forcing allow enough room in spectral space to attain this level within the inertial range is a matter of debate. These concerns are supported by a resolution study that shows substantially larger variation of relative exponents of first-order SFs when grid resolution increases from 512^3 to 1024^3 in models with compressive forcing (≈ 5 per cent) compared to solenoidal ones (≈ 2 per cent, see table II in Schmidt et al. 2008). If the effective Reynolds numbers of compressively driven supersonic turbulence models are substantially smaller than those with natural forcing, then a meaningful comparison of inertial range scaling should involve compressive models with much higher grid resolutions to provide comparable scale separation in the inertial range. This would likely

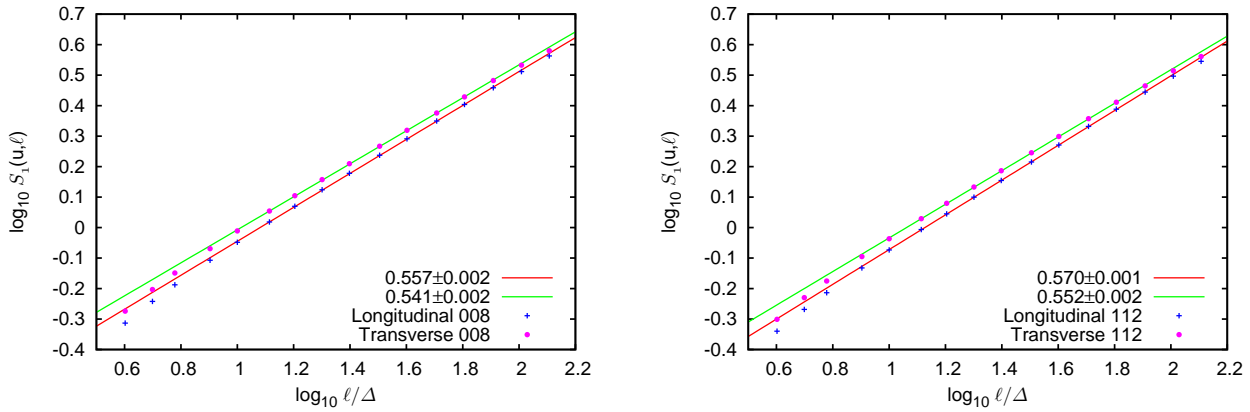


Figure 2. As Fig. 1, but for an AMR simulation with self-gravity, model HD3. The two plots show SF scaling based on the 512^3 root grid information for two flow snapshots. Left-hand panel shows the scaling in fully developed turbulence at $t = 0$ (no self-gravity). Right-hand panel shows the same scaling plot, but for the last flow snapshot at $t = 0.43 t_{\text{ff}}$ (with self-gravity), when a number of collapsing cores are present in the computational domain. Each data point represents an average over $\sim 8 \times 10^8$ velocity difference measurements. Numbers in the legend represent the power-law indices, ζ_1 , for the linear least-squares representation of the data points in the range $\ell/\Delta \in [10, 100]$ and formal uncertainty of the fits. The root grid resolution in this model is $\Delta \simeq 0.01$ pc; the range of scales shown 0.3–1.5 pc.

make such a comparison computationally expensive. Existing computational models with compressive forcing can also be verified using analytical relations for inertial range scaling in supersonic turbulence (Falkovich, Fouxon & Oz 2010; Galtier & Banerjee 2011; Wagner et al. 2012; Aluie 2013; Kritsuk et al. 2013). Since the Reynolds numbers in the ISM are quite large, directly comparing isothermal simulations with exotic forcing at grid resolutions $\lesssim 1024^3$ with observations is difficult due to restrictions imposed by the adopted EOS (cf. Federrath, Klessen & Schmidt 2009; Federrath et al. 2010; Roman-Duval et al. 2011). In this respect, $\zeta_1 \simeq 0.54$ obtained in model HD2 with forcing close to natural better represents the universal trends and thus bears more weight in comparison with relevant observations.

As we have seen, state-of-the-art observations leave substantial freedom of interpretation. In these circumstances, numerical experiments can provide critical tests to verify or invalidate the proposed scenarios. One way to do this is to check the scaling of the velocity SFs in numerical simulations that include self-gravity and see if there is any difference.

3.2 Isothermal models with self-gravity

Here, we use a very high dynamic range simulation of isothermal self-gravitating turbulence with adaptive mesh refinement and effective linear resolution of 5×10^5 (Padoan et al. 2005; Kritsuk et al. 2011b). Our model HD3 is defined by the periodic domain size, $L = 5$ pc, rms Mach number, $M_s = 6$, virial parameter, $\alpha_{\text{vir}} \equiv 5\sigma_u^2 R/(GM) \approx 0.25$ (Bertoldi & McKee 1992), free-fall time, $t_{\text{ff}} \equiv (3\pi/32G\rho)^{1/2} \approx 1.6$ Myr, and dynamical time, $t_{\text{dyn}} \equiv L/(2M_s c_s) \approx 2.3$ Myr. The simulation was initialized as a uniform grid turbulence model by stirring the gas in the computational domain for $4.8t_{\text{dyn}}$ with a large-scale random force that includes 40 per cent dilatational and 60 per cent solenoidal power. After the initial stirring period, which ended at $t = 0$ with a fully developed statistically stationary supersonic turbulence, the forcing was turned off and the model was further evolved with AMR and self-gravity

for about $0.29t_{\text{dyn}} \simeq 0.43t_{\text{ff}}$. We compare scaling of the first order velocity SFs computed for $t = 0$ and $t = 0.43t_{\text{ff}}$ flow snapshots. Fig. 2 illustrates the result: a 1.8 per cent difference in scaling exponents between the non-self-gravitating ($\zeta_1 \simeq 0.55$, left-hand panel) and self-gravitating ($\zeta_1 \simeq 0.56$, right-hand panel) snapshots at the root grid resolution of 512^3 . The difference is small compared to the usual statistical snapshot-to-snapshot variation in turbulence simulations at this resolution.

We clearly see the lack of statistically significant imprints of self-gravity on the velocity scaling, even though by the end of the simulation the peak density has grown by more than eight decades and the density probability density function (PDF) has developed a strong power-law tail at the high end, while the initial lognormal low end of the distribution has shifted to slightly lower densities (Kritsuk et al. 2011b). Similar results were obtained by Collins et al. (2012), who independently demonstrated that in driven MHD turbulence simulations with self-gravity and AMR the velocity power spectra do not show any signs of ongoing core formation, while the density and column density statistics bear a strong gravitational signature on all scales. The absence of a significant signature of gravity in the velocity statistics can be readily understood as the local velocity gains due to gravitational acceleration are simply insufficient to be seen on the background of supersonic turbulent fluctuations supported by the large-scale kinetic energy injection during the stirring period.

We believe it is clear enough that as far as the inner velocity structure of MCs is concerned, it is obviously shaped by the turbulence. If there is a contribution from gravity, it is relatively small. The larger scale velocity picture can nevertheless bear more complexity, in particular at scales approaching the ‘full 3D system size’ or the effective energy injection scale of ISM turbulence, which is believed to be close to the (cold) gaseous disc scaleheight. There, the formation of coherent, possibly gravitationally bound structures in an essentially two-dimensional setting of a differentially rotating disc would perhaps dominate over the seeds of

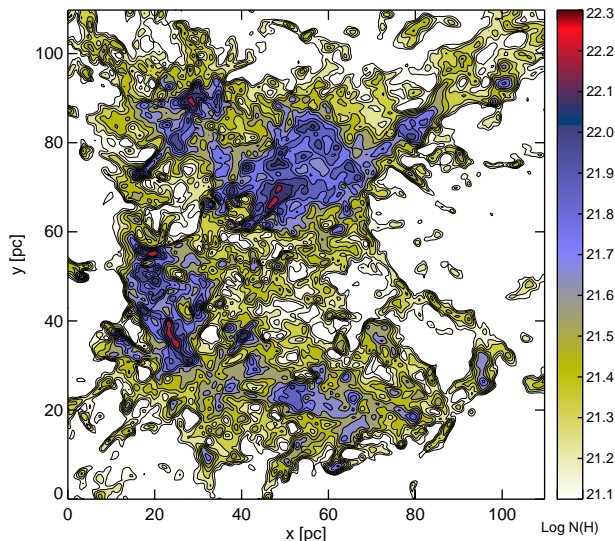


Figure 3. A synthetic contour map of projected density distribution for the cold gas ($T < 184$ K) in a subvolume of the $(200 \text{ pc})^3$ computational domain in the multiphase MHD turbulence model MD2 representing a simulated equivalent of an MC complex. The original grid resolution of the snapshot, $\Delta = 0.39$ pc, has been coarsened by a factor of ~ 3 to match the 0.5° angular resolution of the historical ^{12}CO map of MCs in Perseus, Taurus, and Auriga published 25 years ago by Ungerechts & Thaddeus (1987). The morphology of contours closely resembles the observations. Colour bar indicates the logarithm of column density of cold material.

direct three-dimensional turbulent energy cascade entering the inertial range.

Isothermal simulations HD1, HD2, and HD3 were designed to model the structure of MCs on scales $\lesssim 5$ pc powered by the cascade coming from larger scales ~ 100 pc, where this energy is injected by stellar feedback, galactic shear, gas infall on to the disc, etc. We have shown that isothermal models successfully reproduce the power index in the observed linewidth–size relation. We have also shown that self-gravity of the turbulent molecular gas, while actively operating on scales $\lesssim 1$ pc, does not produce a measurable signal in the linewidth–size relation. This suggests that the turbulence alone might indeed be responsible for the first Larson law, as observed within MCs, with a caveat that the coefficient in the relation cannot be predicted by the scale-free isothermal simulations by their design. Since an isothermal approximation we used so far cannot be justified for models of larger scale MC structure, we designed a numerical experiment that would properly model the ISM thermodynamics and allow us to define a reasonable proxy for the cold molecular gas traced by CO observations.

3.3 Multiphase models

A suite of such numerical simulations, which also include an approximation for the cooling and heating functions (Wolfire et al. 1995) and magnetic field, but ignore self-gravity and local feedback from star formation, is described in section 3 of Kritsuk, Ustyugov & Norman (2011a). Here, we shall mostly discuss model MD2, a moderately magne-

tized case, with a domain size $L = 200$ pc, mean hydrogen number density $n = 5 \text{ cm}^{-3}$, uniform magnetic field $B_0 = 3 \mu\text{G}$ and a solenoidal random force acting on scales between 100 and 200 pc. The force is normalized to match the width of the mass-weighted PDF of thermal pressure in the diffuse cold medium of the Milky Way recovered from the *Hubble Space Telescope* observations (Jenkins & Tripp 2011; Kritsuk et al. 2011a). The model was evolved for ~ 60 Myr (the dynamical time for model MD2 $t_{\text{dyn}} = L/2u_{\text{rms}} \simeq 6.1$ Myr) from uniform initial conditions and the final stretch of ~ 25 Myr represents an established statistical steady state with an rms magnetic field strength $B_{\text{rms}} \simeq 11.7 \mu\text{G}$ and with ~ 51 per cent of the total gas mass $M_{\text{tot}} = 9.2 \times 10^5 M_\odot$ residing in the thermally stable cold phase at temperatures $T \lesssim 184$ K.

Fig. 3 shows a synthetic column density map of what observationally would be classified as an MC complex, morphologically resembling clouds in Perseus, Taurus, and Auriga observed in CO (Ungerechts & Thaddeus 1987). The map covers the cold gas in a projected area of ~ 30 per cent of a full 2D flow snapshot. With a set of ~ 70 snapshots available for this model, one can easily track the formation, evolution, and breakdown of structure in the MC complex over a few 10^7 years. While in projection the mapped MCs may look like quasi-uniform clouds with well-defined boundaries, the dense cold clumps of gas in the simulation box actually fill only a small fraction of their volume (~ 7 per cent overall), similar to what observations suggest (e.g. Blitz 1987). In three dimensions, the clouds represent a collection of mostly disjoint, under-resolved structures that randomly overlap in projection. As these structures move supersonically, the physical identity (in the Lagrangian sense) of the ‘clouds’ we see in projection is actively evolving. This makes simplified scenarios often discussed in the literature, which imply isolated static clouds (e.g. a collision of two clouds or collapse of an isolated cloud) or converging flows taken out of the larger-scale turbulence context very unrealistic. The so-called interclump medium (ICM; e.g. Hennebelle & Falgarone 2012) is mostly composed of thermally unstable gas at intermediate temperatures (Field 1965; Hunter 1970; Heiles 2001; Kritsuk & Norman 2002). The ICM comprises ~ 70 per cent of the whole volume of the computational domain and ~ 23 per cent is filled with the stable warm phase at $T \gtrsim 5250$ K. Phase transformations are quite common in such multiphase environments with individual fluid elements actively cycling through various thermal states in response to shocks and patches of supersonic velocity shear.

Turbulence models of this type bear substantially more complexity since different thermal phases represent different physical regimes – from supersonic and super-Alfvénic in the cold phase, including the molecular gas, ($M_s \simeq 15.2$, $M_A \simeq 4.2$) to transonic and trans-Alfvénic in the warm phase ($M_s \simeq 1.7$, $M_A \simeq 1.2$). Active baroclinic vorticity creation fosters exchange between compressible kinetic and thermal modes otherwise suppressed by kinetic helicity conservation enforced in isothermal turbulence (Kritsuk & Norman 2002; Elmegreen & Scalo 2004). This rich diversity ultimately determines velocity scaling and other statistical properties of multiphase turbulence (Kritsuk & Norman 2004).

In order to check if model MD2 will reproduce the velocity scaling recovered from observations of tracers of the cold gas, such as ^{12}CO or ^{13}CO , we can calculate velocity

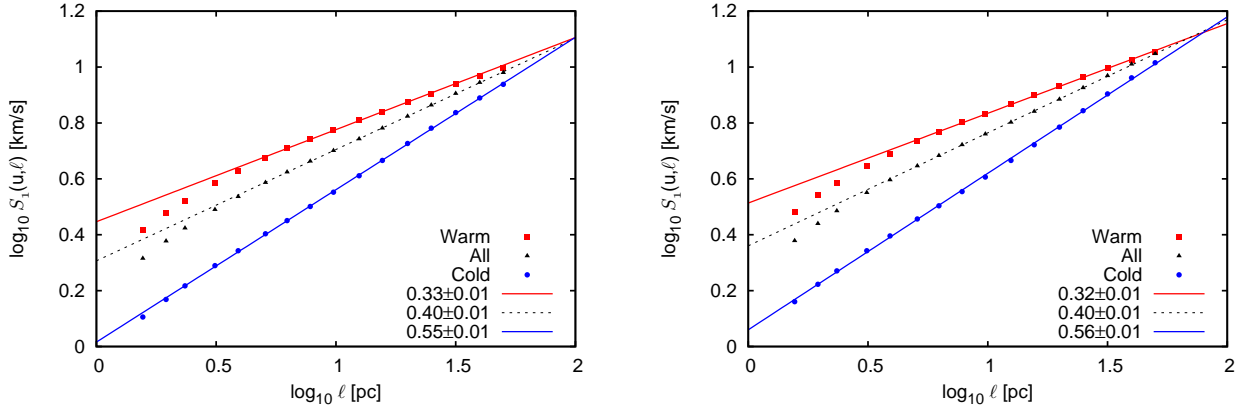


Figure 4. First-order longitudinal (left) and transverse (right) velocity SFs based on the 512^3 multiphase MHD turbulence simulation. Triangles represent SFs for the whole domain; squares represent two-point correlations conditioned for the warm stable phase with temperatures $T > 5250$ K that fills ~ 23 per cent of the volume; circles represent SFs conditioned for the cold phase with $T < 184$ K that occupies ~ 7 per cent by volume and contains ~ 50 per cent of the mass. Each triangle represents an average over $\sim 6 \times 10^{10}$ velocity difference measurements in ~ 70 flow snapshots covering $\sim 4 t_{\text{dyn}}$ or ~ 25 Myr of statistically steady evolution. Numbers in the legend represent the power-law indices, ζ_1 , for the linear least-squares representation of the data points and the formal uncertainty of the fits.

SFs conditioned on the cold phase only, i.e. all velocity differences entering the ensemble average will be measured for point pairs located in the cold gas only. While a detailed knowledge of CO chemistry is needed to connect models and observations, this simplified approach can be used as the first step from isothermal models to more sophisticated and costly numerical simulations with complex interstellar chemistry.

Fig. 4 shows time-averaged first-order SFs of longitudinal (left) and transverse (right) velocity in the statistically stationary regime of model MD2. Black triangles indicate SFs for point pairs selected from the whole volume following the same procedure as in Figs 1 and 2. The scaling exponent $\zeta_{1,\text{all}} \simeq 0.4$ is somewhat larger than the Kolmogorov value of $1/3$ as most of the volume is filled with mildly supersonic thermally unstable gas ($M_s \simeq 4.2$). Red triangles show SFs conditioned on the warm stable phase only. Since the warm phase is essentially transonic, the velocity scaling is very close to Kolmogorov’s, $\zeta_{1,\text{warm}} \simeq 0.33$. Blue circles indicate SFs conditioned on the cold, thermally stable, strongly supersonic phase. The exponents, $\zeta_{1,\text{cold}} \simeq 0.56$, measured in the range $\ell \in [1.5, 50]$ pc are consistent with the results of CO observations we discussed earlier in this section.

The slope of the correlation is only weakly sensitive to the magnetization level assumed in the model. Model MD3 has $B_0 = 9.5 \mu\text{G}$, $B_{\text{rms}} \simeq 16 \mu\text{G}$ and $\zeta_{1,\text{cold}} \simeq 0.52$, while model MD1 has $B_0 = 1 \mu\text{G}$, $B_{\text{rms}} \simeq 8 \mu\text{G}$ and $\zeta_{1,\text{cold}} \simeq 0.65$.

An interesting feature of the velocity scaling in the cold gas (circles in Fig. 4) – which still needs to be understood – is the extent of the power law into the range of scales where numerical dissipation usually plays a role and its effects are clearly seen in the unconditional SF scaling (triangles) and in the scaling for the warm gas (squares). Even though the number of point pairs in the cold phase is limited due to the small volume fraction of the phase, the scaling is still reasonably well defined statistically due to the large number of flow snapshots involved in the averaging.

Another important feature of the cold gas velocity scaling is the value of the coefficient $u_0(1 \text{ pc}) \sim 1 \text{ km s}^{-1}$ in

models MD1, MD2 and MD3, independent of the magnetization level. This value roughly matches the observationally determined coefficient in the linewidth–size relation. As we mentioned above, the rms velocity in the box is controlled by the forcing normalization and by the mean density of the gas. These values were chosen to match the observed distribution of thermal pressure, which is only weakly sensitive to the magnetic effects. A much weaker or stronger forcing would change the rms velocity and the coefficient, but then the pressure distribution would not match the observations, see for instance model E in Kritsuk et al. (2011a).

Finally, while near the energy injection scale ~ 100 pc the velocity correlations for different thermal phases show the same amplitude, there is a clear difference in the SF levels for the cold and warm gas in the inertial range. Due to the difference in SF slopes at different Mach number regimes probed, the warm gas shows progressively higher velocity differences than the cold gas at lower length-scales. For instance, at $\ell = 10$ pc the ratio $\langle |\delta u_{\text{cold}}| \rangle / \langle |\delta u_{\text{warm}}| \rangle \sim 0.6$. Our multiphase models only allow for a quite broad definition of the cold phase based on the temperature threshold determined by the thermal stability criterion (Field 1965). However one can imagine that observations of molecular gas tracers with different effective temperatures and densities would quite naturally provide different estimates for the velocity dispersion as a function of scale. This would in turn lead to different virial parameters probed by different traces with the net result of clouds observed using lower opacity traces to *appear* more strongly bound (e.g. Koda et al. 2006).

As a quick summary of the results so far, we have seen that numerical simulations of interstellar turbulence can successfully reproduce the observed linewidth–size relation including both the coefficient and the slope. Self-gravity of the gas does not seem to produce any significant modifications to the scaling relation over the range of scales simulated. Our isothermal models HD1–3 cover the range of scales from about 2 pc down to 0.3 pc, while the multiphase models MD1–3 extend this range to ~ 50 pc.

4 THE MASS–SIZE RELATION

An alternative formulation of the original Larson's third law, $m \propto L^{1.9}$, implied a nested hierarchical density structure in MCs. Such a concept was proposed by von Hoerner (1951) (see also von Weizsäcker 1951) to describe an intricate statistical mixture of shock waves in highly compressible interstellar turbulence. He pictured density fluctuations as a hierarchy of interstellar clouds, analogous to eddies in incompressible turbulence. Observations indeed reveal a pervasive 'fractal' structure in the interstellar gas that is usually interpreted as a signature of turbulence (Falgarone & Phillips 1991; Elmegreen & Falgarone 1996; Lequeux 2005; Roman-Duval et al. 2010; Hennebelle & Falgarone 2012). Numerous attempts to measure the actual Hausdorff dimension of the MC structure either observationally or in simulations demonstrated that such measurements are notoriously difficult and bear substantial uncertainty, which depends on what measure is actually used. Here, we narrow down the discussion solely to the so-called mass dimension, i.e. the power index in the third Larson law.

The most recent result for a sample of 580 MCs, which includes the SRBY87 clouds, shows a very tight correlation between cloud radii and masses,

$$m(R) = (228 \pm 18M_{\odot})R^{2.36 \pm 0.04}, \quad (4)$$

for $R \in [0.2, 50]$ pc (Roman-Duval et al. 2010). The power-law exponent in this relation, $d_m \approx 2.36$, corresponds to a 'spongy' medium organized by turbulence into a multi-scale pattern of clustered corrugated shock-compressed layers (Kritsuk et al. 2006b). Note, that $d_m \approx 2.36$ under a reasonable assumption of anisotropy implies $\Sigma \propto mL^{-2} \propto L^{0.36}$. Thus, the observed mass–size correlation does not support the idea of a universal mass surface density of MCs. Meanwhile, a positive correlation of Σ with ℓ removes the theoretical objections against the third Larson law outlined in Section 1.

Direct measurements of d_m in the simulations give the inertial subrange values in good agreement with observations: $d_m = 2.39 \pm 0.01$ (model HD2) and 2.28 ± 0.01 (model HD1; Fig. 5). Note that ± 0.01 represents the formal uncertainty of the fit, not the actual uncertainty of d_m , which is better characterized by the difference between the two independent simulations and lies somewhere within $\pm(5-10)$ per cent of d_m . Federrath et al. (2009) obtained $d_m \simeq 2.11$ and 2.03 from two 1024^3 simulations with purely solenoidal and compressive forcing, respectively (see their fig. 7). Their result for solenoidal forcing is broadly consistent with our measurement for a larger 2048^3 simulation within the uncertainty of the measurement. However, their model with a purely compressive forcing rendered a lower mass dimension value of 2.03 , while it is expected to be larger for this type of forcing. A detailed inspection of fig. 7 in Federrath et al. (2009) shows that the scaling range $d_m(\ell) = \text{const.}$ for this model is quite short or nonexistent making this measurement very uncertain. This further indicates that concerns about insufficient scale separation in numerical simulations with purely compressive forcing (see Section 3.1) are valid.

An accurate measurement of d_m in numerical simulations of supersonic turbulence requires extensive statistical sampling since the density (unlike the velocity) experiences

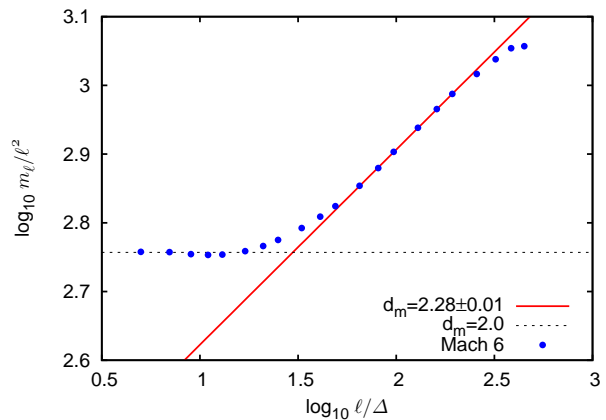


Figure 5. Compensated scaling of the mass, m_{ℓ} , with size ℓ in model HD1. Dissipation-scale structures are shocks with $d_m \simeq 2$. Inertial-range structures have $d_m \simeq 2.3$.

huge spatial and temporal fluctuations. Because of that, only the highest resolution simulations with sufficient scale separation can yield reliable estimates of d_m . We have shown above that, like ζ_1 , the mass dimension also depends on forcing. However, as we discussed in Section 3.1, the non-linear coupling of dilatational and solenoidal modes in compressible turbulence provides certain constraints on the artificial forcing employed in isothermal simulations (Kritsuk et al. 2010). Therefore, the higher end values of mass dimension $d_m \simeq 2.4$ recovered from simulations of supersonic turbulence with forcing close to natural seem more realistic.

Observations of Roman-Duval et al. (2010) represent perhaps the most extended sample of local clouds available in the literature (for ^{12}CO data compilations covering a wider Galactic volume and range of size scales $0.005 \lesssim L \lesssim 200$ pc, see Lequeux 2005; Hennebelle & Falgarone 2012).

With $d_m \simeq 2.36$, the power-law index in the linewidth–size relation compatible with the virial equilibrium condition (1), $\zeta_{1,\text{vir}} \equiv (d_m - 1)/2 \simeq 0.68$, is still reasonably close to the scaling exponent $\zeta_1 \simeq 0.56$ in equation (3), even if one assumes $u_0 = \text{const.}$ (see Section 5.1 below). Thus, we cannot exclude the possibility of virial equilibrium (or kinetic/gravitational energy equipartition, see Ballesteros-Paredes 2006) across the scale range of several decades based on the available observations alone. However, if one adopts the virial interpretation of Larson's laws, the origin of the mass–size correlation observed over a wide range of scales remains unclear. The turbulent interpretation does not have this problem as the slopes of both linewidth–size and mass–size correlations are readily reproduced in simulations and can be predicted for the Kolmogorov-like cascade picture using dimensional arguments, see Section 5. Moreover, the two slopes in the cascade picture are algebraically coupled and this connection is supported observationally, as well as the inertial cascade picture itself (Hennebelle & Falgarone 2012).

5 INTERSTELLAR TURBULENCE AND LARSON'S LAWS

In the absence of a simple conceptual theory of supersonic turbulence, many important questions related to the structure and kinematics of MCs remained unanswered. One of them is the applicability of the universality concept to MC turbulence. The other related question is which of Larson's laws is fundamental? We briefly review the current theoretical understanding of universal properties of turbulence and address these two basic questions below using a phenomenological approach.

5.1 Universality in incompressible turbulence

Before we generalize our discussion to turbulence in compressible fluids, it is instructive to briefly review the notion of universality as it was first introduced for incompressible fluids. In turbulence research, universality implies independence of scaling on the particular mechanism by which the turbulence is generated (e.g. Frisch 1995). Assuming homogeneity, isotropy and finiteness of the energy dissipation rate in the limit of infinite Reynolds numbers, $Re \equiv \ell_0 u_0 / \nu \rightarrow \infty$, Kolmogorov (1941a,b) derived the following exact relation from the N-S equation

$$S_{3,\parallel}(u, \ell) \equiv \langle (\delta u_{\parallel, \ell})^3 \rangle = -\frac{4}{5} \varepsilon \ell, \quad (5)$$

known as the four-fifths law. Here, $\delta u_{\parallel, \ell}$ is the longitudinal velocity increment

$$\delta u_{\parallel, \ell} = [\mathbf{u}(\mathbf{x} + \boldsymbol{\ell}) - \mathbf{u}(\mathbf{x})] \cdot \boldsymbol{\ell} / \ell, \quad (6)$$

ε is the mean energy dissipation rate per unit mass and equation (5) holds in the inertial subrange of scales $\eta \ll \ell \ll \ell_0$, where the direct influence of energy injection at $\ell_0 \rightarrow \infty$ and dissipation at the Kolmogorov scale $\eta \equiv (\nu^3 / \varepsilon)^{1/4}$ can be neglected. The four-fifths law is essentially a statement of conservation of energy in the inertial range of a turbulent fluid, while $S_{3,\parallel}(u, \ell) / \ell$ is an indirect measure of the energy flux through spatial scale ℓ , corresponding to the Richardson (1922) picture of the inertial energy cascade. Assuming further that the cascade proceeds in a self-similar way, the K41 theory predicted a general scaling for p th order SFs

$$S_p(u, \ell) = C_p \varepsilon^{p/3} \ell^{p/3}, \quad (7)$$

where the constants C_p are dimensionless. A particular case of equation (7) with $p = 2$ leads to the famous Kolmogorov–Obukhov energy spectrum

$$P(u, k) = C_K \varepsilon^{2/3} k^{-5/3}, \quad (8)$$

where $k \equiv 2\pi / \ell$ is the wavenumber and C_K is the Kolmogorov constant. The slope of the spectrum $\beta = 5/3$ is related to the slope of the second order SF $\zeta_2 = 2/3$ since one is the Fourier transform of the other and therefore

$$\beta = \zeta_2 + 1. \quad (9)$$

Likewise, if the self-similarity holds true, then equation (9) can be used to obtain the slope of the first-order SF as a function of the power spectrum slope

$$\zeta_1 = (\beta - 1) / 2. \quad (10)$$

The self-similarity hypothesis implies that the statistics of velocity increments in equation (7) are fully determined by the universal constants C_p and C_K , and depend only on the energy injection rate $\varepsilon > 0$ and the lag ℓ . This prediction, however, was challenged by Landau in 1942 (Landau & Lifshitz 1987, section 38, p. 140) and did not receive experimental support (for orders p other than 3), eventually leading to the formulation of the refined similarity hypothesis (RSH)

$$S_p(u, \ell) = C_p \langle \varepsilon_\ell^{p/3} \rangle \ell^{p/3} \propto \ell^{\zeta_p}, \quad (11)$$

(where $\zeta_p = p/3 + \tau_{p/3}$) to account for the inertial range intermittency (Kolmogorov 1962). A hierarchical structure model based on the RSH and on the assumption of log-Poisson statistics of the dissipation field ε_ℓ (She & Leveque 1994; Dubrulle 1994) successfully predicted the values of anomalous scaling exponents ζ_p measured in large-scale direct numerical simulations (DNS). Recently obtained DNS data at large, but finite Reynolds numbers support the universal nature of anomalous exponents ζ_p in the spirit of K41, but including relatively small intermittency corrections $\tau_p \neq 0$ for orders p at least up to $p = 8$, except $\tau_3 = 0$ (Gotoh 2002; Ishihara et al. 2009). The DNS results also show that the slope of the energy spectrum compensated with $k^{5/3}$ is slightly tilted, suggesting that $P(u, k) \propto k^{-5/3+\phi}$ with $\phi = -0.1$ (Kaneda et al. 2003). Whether the constants C_p and $C_K = 1.6 \pm 0.1$ are universal or not still remains to be seen (for references see Ishihara et al. 2009).

5.2 Universal properties of supersonic turbulence

As far as compressible fluids are concerned, up until recently there were no exact relations similar to the four-fifths law (5) available. However, the growing body of theoretical work (Falkovich et al. 2010; Galtier & Banerjee 2011; Aluie 2011; Aluie et al. 2012; Wagner et al. 2012; Banerjee & Galtier 2013; Aluie 2013) now supports the existence of a Kolmogorov-like inertial energy cascade in turbulent compressible fluids suggested earlier by phenomenological approaches (Henriksen 1991; Fleck 1996; Kritsuk et al. 2007a).

For the extreme case of supersonic turbulence in an isothermal fluid, which represents a simple model of particular interest for MCs, an analogue of the four-fifths law was obtained and verified with numerical simulations (Kritsuk et al. 2013)

$$\langle \delta(\rho \mathbf{u}) \cdot \delta \mathbf{u} \delta u_{\parallel} + [\delta(d\rho \mathbf{u}) - \tilde{\delta} d \delta(\rho \mathbf{u})] \cdot \delta \mathbf{u} \rangle \simeq -\frac{4}{3} \rho_0 \varepsilon \ell, \quad (12)$$

where $d \equiv \nabla \cdot \mathbf{u}$ is the dilatation, $\tilde{\delta} d \equiv d(\mathbf{x} + \boldsymbol{\ell}) + d(\mathbf{x})$, ε has the same meaning as in equation (5), and ρ_0 is the mean density. This relation follows from a more involved exact relation derived from the compressible N-S equation using an isothermal closure (Galtier & Banerjee 2011). It further reduces to a primitive form of equation (5) in the incompressible limit,

$$\langle (\delta \mathbf{u})^2 \delta u_{\parallel} \rangle = -\frac{4}{3} \varepsilon \ell, \quad (13)$$

when $\rho \equiv \rho_0$ and $d \equiv 0$.

At Mach 6 typical for the MC conditions, the first term on the l.h.s. of equation (12) representing the inertial flux

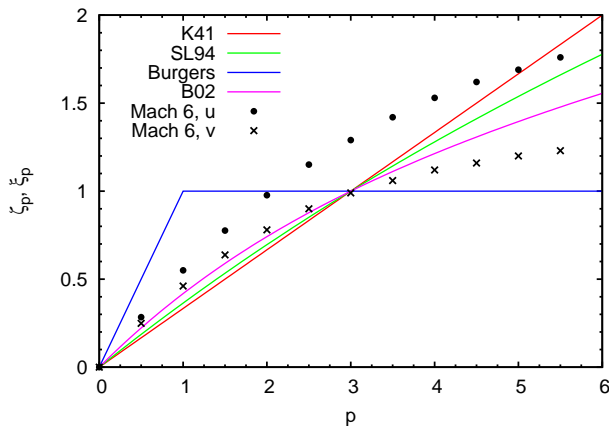


Figure 6. Absolute scaling exponents for SFs of transverse velocity [$S_p(u, \ell) \propto \ell^{\zeta_p}$, circles] and density-weighted velocity $v = \rho^{1/3}u$ [$S_p(v, \ell) \propto \ell^{\zeta_p}$, crosses] for model HD2. Solid lines show ζ_p predicted by the K41 theory (red), Burgers model (blue), and intermittency models due to She & Leveque (1994, green) and Boldyrev (2002, magenta). Note that the Burgers model predicts $\zeta_1 = 1$ rather than $\zeta_1 = 1/2$ (cf. McKee & Ostriker 2007).

of kinetic energy is negative and a factor of ≈ 3 larger in absolute value than the sum of the second and third terms describing an energy source associated with compression/dilatation. Numerical results show that both flux and source terms can be approximated as linear functions of the separation ℓ in the inertial range. Hence, equation (12) reduces to

$$\langle \delta(\rho \mathbf{u}) \cdot \delta \mathbf{u} \delta u_{\parallel} \rangle \simeq -\frac{4}{3} \rho_0 \varepsilon_{\text{eff}} \ell, \quad (14)$$

where the effective energy injection rate ε_{eff} includes the source contribution. Comparing equations (13) and (14) one can see that strong compressibility in supersonic turbulence is ultimately accounted for by the presence of the momentum density increment in the l.h.s. of equation (14) and also formally requires a compressible correction to the mean energy injection rate.

A simplified formulation of equation (14) based on dimensional analysis

$$S_3(v, \ell) \equiv \langle |\delta v|^3 \rangle \propto \ell, \quad (15)$$

where $\mathbf{v} \equiv \rho^{1/3} \mathbf{u}$, was introduced in Kritsuk et al. (2007a,b) and its linear scaling was further verified with numerical simulations in a wide range of Mach numbers (Kowal & Lazarian 2007; Schwarz et al. 2010; Zrake & MacFadyen 2012). Note that a ‘symmetric’ density weighting in the third-order SF (15) differs from the original form in the l.h.s. of equation (14), which includes momentum and velocity differences, and that the absolute value of the increment is taken in equation (15). While the linear scaling is preserved in equation (15) for absolute values of both longitudinal and transverse differences of \mathbf{v} , the extent of the scaling range is substantially shorter compared to that seen in equation (14) for the same numerical model (Kritsuk et al. 2013).

Finally, using (15) and following an analogy to K41, one can also postulate self-similarity of the energy cascade

in supersonic turbulence and predict a general scaling for the p th order SFs of the mass-weighted velocity

$$S_p(v, \ell) \equiv \langle |\delta v|^p \rangle \propto \ell^{p/3} \quad (16)$$

and for the power spectrum

$$P(v, k) \propto k^{-5/3}. \quad (17)$$

While scaling relations (16) and (17) generally reduce to (7) and (8) in the incompressible limit, it is hard to expect them to universally hold in compressible fluids for the following two reasons: First, as we have seen in § 5.1, even in incompressible fluid flows, relations (7) and (8) are not strictly universal due to intermittency (except for $p = 3$). Secondly, the transition from relationship (12) to (15) involves a chain of non-trivial assumptions that can potentially influence (or even eliminate) the scaling. A combination of these two factors can produce different results depending on the nature of the large-scale energy source for the turbulence.

Nevertheless, the power spectra of \mathbf{v} demonstrated Kolmogorov-like slopes $\beta \approx 5/3$ in numerical simulations at moderately high Reynolds numbers, suggesting that intermittency corrections should be somewhat larger than in the incompressible case, but still reasonably small at $p = 2$ (Kritsuk et al. 2007a,b; Schmidt et al. 2008; Federrath et al. 2010; Price & Federrath 2010). For instance, the ‘world’s largest simulation’ of supersonic ($M = 17$) turbulence with numerical resolution of 4096^3 mesh points and a large-scale solenoidal forcing gives $P(v, k) \propto k^{-5/3+\psi}$ with $\psi = -0.07$ (Federrath 2013), which shows an intermittency correction ψ similar to $\phi = -0.1$ seen in the incompressible DNS of comparable size (Kaneda et al. 2003).

In a twin 4096^3 simulation with purely compressive forcing limited to $k/k_{\text{max}} \in [1, 3]$, Federrath (2013) finds a steep scaling range with $P(v, k) \propto k^{-2.1}$ at $k/k_{\text{max}} \in [12, 30]$, which then flattens to $-5/3$ at $k/k_{\text{max}} \in [40, 50]$ shortly before entering the so-called ‘bottleneck’ range of wavenumbers. It is not clear where the inertial range is in this case since detailed analysis of the key correlations in relation (12) is lacking. Visual inspection of flow fields in this simulation indicates the presence of strong coherent structures associated with the large-scale energy injection, which can be responsible for the -2.1 scaling. It seems likely that in the extreme case of purely compressive stirring, the mean energy injection is substantially less localized to the large scales due to the nature of non-linear energy exchange between the dilatational and solenoidal modes (Moyal 1952), resulting in a substantially shorter inertial range (see also Kritsuk et al. 2010; Wagner et al. 2012; Aluie 2013; Kritsuk et al. 2013). A factor of ≈ 4 lower level of enstrophy in this model compared to the one with solenoidal forcing implies a lower value of the effective Reynolds number, also symptomatic of a shorter inertial range.

Fig. 6 shows how the absolute scaling exponents of SFs of \mathbf{u} and \mathbf{v} vary with the order p in model HD2 at $M_s = 6$. Filled circles show exponents ζ_p of the velocity SFs for $p \in [0.5, 5.5]$. In subsonic or transonic regimes these exponents would closely follow the K41 prediction $\zeta_p = p/3$, if isotropy and homogeneity were assumed and intermittency ignored. Starting from $M_s \gtrsim 3$, however, ζ_3 shows a clear excess over unity that gradually increases with the Mach number, indicating a non-universal trend. For the density-

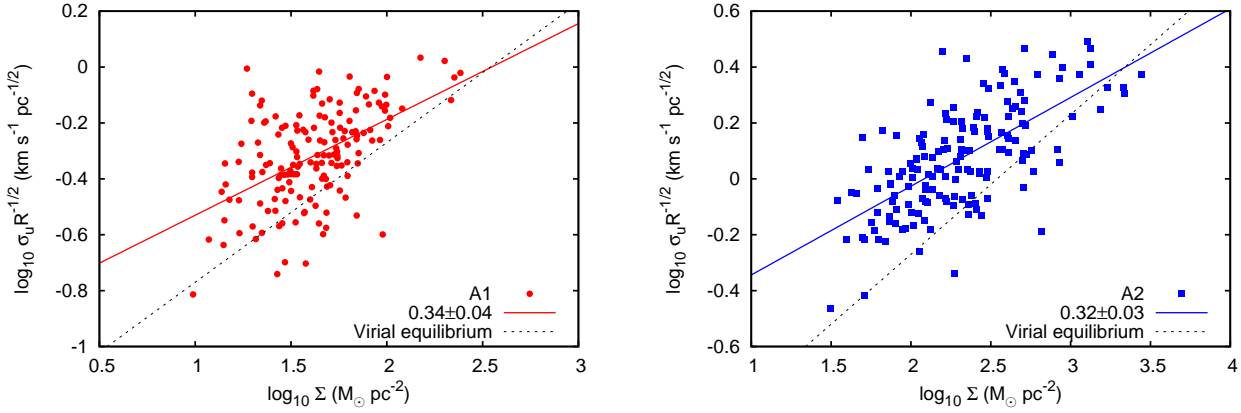


Figure 7. Variation of the scaling coefficient $u'_0 = \sigma_u R^{-1/2}$ with mass surface density Σ based on data from Heyer et al. (2009). Solid lines with slopes 0.34 ± 0.04 and 0.32 ± 0.03 show linear least-squares fits to A1 (left) and A2 (right) subsets from Heyer et al. (2009), respectively. Dashed line in both cases shows the correlation expected for clouds in virial equilibrium.

weighted velocity \mathbf{v} , the slope of the third-order SF, $\xi_3 \approx 1$, does not depend on the Mach number, while ξ_p at $p \neq 3$ demonstrate an anomalous scaling that is successfully predicted by the hierarchical structure model of She & Leveque (1994), although with parameters that differ from those for the incompressible case and from those suggested by Boldyrev (2002) for relative exponents ζ_p/ζ_3 (Kritsuk et al. 2007b; Pan et al. 2009). Note that supersonic turbulence is more intermittent than incompressible turbulence, since the crosses in Fig. 6 deviate stronger from the K41 prediction than the green line corresponding to the She–Leveque model. For orders $p = 1$ and 2 of particular interest to this work, corrections $\tau_{p/3}$ appear to be relatively small.

Our discussion above demonstrates the non-universal nature of scaling relation (3), while showing that a universal scaling is expected for the fourth-order correlations described by the l.h.s. of equation (14) as well as for a dimensionally equivalent form (15). The first- and second-order statistics of \mathbf{v} depend on the relatively small intermittency corrections, $\xi_p = p/3 + \tau_{p/3}$ at $p = 1, 2$. It is hard to tell whether the anomalous scaling exponents ξ_p are universal in the limit of infinitely large Reynolds numbers (as ζ_p in the case of incompressible turbulence) or not. Carefully designed large-scale numerical simulations will help to improve our understanding of intermittency in supersonic turbulence and address this important question.

5.3 The turbulent origin of Larson’s laws

Is there any direct observational evidence supporting the turbulent origin of the non-thermal velocity fluctuations in MCs? Do we see any indication that the fundamental relation (14) is satisfied? Indeed, the fact that the rate of energy transfer per unit volume in the inertial cascade, $\epsilon_\ell \equiv \rho_\ell u_\ell^3/\ell$, is roughly the same in three different components of the cold neutral medium: in the cold HI, in MCs, and in dense molecular cores (Lequeux 2005), strongly suggests that the energy propagates across scales in a universal way consistent with equation (14). A more recent compilation of ^{12}CO data for the whole population of MCs indicates that ϵ_ℓ shows no variation from structures of ~ 0.01 pc to GMCs of ~ 100 pc

and has the same value observed in the HI gas (fig. 6 in Hennebelle & Falgarone 2012). Although the dispersion of ϵ_ℓ is equally large at all scales, this result suggests that MCs traced by $^{12}\text{CO}(1-0)$ are part of the same turbulent cascade as the atomic ISM.

In the following, we shall exploit the linear scaling of the third-order moment of $\delta\mathbf{v}$, which according to equation (14) implies a constant kinetic energy density flux within the inertial range.

We shall first derive several secondary scaling laws involving the coarse-grained surface density Σ_ℓ , assuming that the effective kinetic energy density flux is approximately constant within the inertial range (and neglecting gravity). Dimensionally, the constant spectral energy flux condition,

$$\rho_\ell (\delta u_\ell)^3 \ell^{-1} \propto \Sigma_\ell (\delta u_\ell)^3 \ell^{-2} \propto \Sigma_\ell \ell^{3\zeta_1 - 2} \approx \text{const.}, \quad (18)$$

implies

$$\Sigma_\ell \propto \ell^{2-3\zeta_1}. \quad (19)$$

Substituting $\zeta_1 = 0.56 \pm 0.02$, as measured by Heyer & Brunt (2004), we get $\Sigma_\ell \propto \ell^{0.32 \pm 0.06}$. We can also rely on the ‘fractal’ properties of the density distribution to evaluate the scaling of Σ_ℓ with ℓ : $\Sigma_\ell \propto \rho_\ell \ell \propto m_\ell/\ell^2 \propto \ell^{d_m - 2}$, which in turn implies $\Sigma_\ell \propto \ell^{0.36 \pm 0.04}$ for $d_m = 2.36 \pm 0.04$ from Roman-Duval et al. (2010). Note that both independent estimates for the scaling of Σ_ℓ with ℓ agree with each other within one sigma. The observations, thus, indicate that mass surface density of MCs indeed positively correlates with their size with a scaling exponent $\sim 1/3$, which is consistent with both velocity scaling and self-similar structure of the mass distribution in MCs.

Let us now examine data sets A1 and A2 presented in Heyer et al. (2009) for a possible correlation of $u'_0 = \sigma_u R^{-1/2}$ with $\Sigma = m/\pi R^2$. The A1 data points correspond to clouds with their original SRBY87 cloud boundaries, while A2 represents the same set of clouds with area within the half-power isophote of the H_2 column density. Figure 7 shows the data and formal linear least-squares fits with slopes 0.34 ± 0.04 and 0.32 ± 0.03 for A1 (left) and A2 (right), respectively. First, note that the Pearson correlation coefficients are relatively small, $r = 0.524$ for A1 and $r = 0.673$ for A2, indicating that the overall quality of

the fits is not very high. Also note that both correlations are formally not as steep as the virial equilibrium condition (1) would imply. At the same time, when the two data sets are plotted together (as in fig. 7 of Heyer et al. 2009) the apparent shift between A1 and A2 data points caused by the different cloud area definitions in A1 and A2 creates an *impression* of virial equilibrium condition being satisfied. An offset of A1 and A2 points with respect to the dotted line is interpreted by Heyer et al. (2009) as a consequence of LTE-based cloud mass underestimating real masses of the sampled clouds. Each of the two data sets, however, suggest scaling with a slope around 1/3 with larger clouds of higher mass surface density being potentially closer to virial equilibrium than smaller structures. The same tendency can be traced in the Bolatto et al. (2008) sample of extragalactic GMCs (Heyer et al. 2009, fig. 8). A similar trend is recovered by Goodman et al. (2009) in the L1448 cloud, where a fraction of self-gravitating material obtained from dendrogram analysis shows a clear dependence on scale. While most of the emission from the L1448 region is contained in large-scale ‘bound’ structures, only a low fraction of smaller objects appear self-gravitating.

Let us check a different hypothesis, namely whether the observed scaling $\sigma_u R^{-1/2} \propto \Sigma^{1/3}$ is compatible with the inertial energy cascade phenomenology and with the observed hierarchical structure of MCs. The constant spectral energy flux condition, $\rho_\ell (\delta u_\ell)^3 \ell^{-1} \approx \text{const.}$, can be recast in terms of $\Sigma_\ell \propto \rho_\ell \ell$ assuming $\delta u_\ell \ell^{-1/2} \propto \Sigma_\ell^\alpha$ with $\alpha \approx 1/3$ and $\rho_\ell \propto \ell^{d_m-3}$,

$$\rho_\ell (\delta u_\ell)^3 \ell^{-1} \propto \rho_\ell \Sigma_\ell \ell^{3/2} \ell^{-1} \propto \ell^{2(d_m-3)+3/2} \approx \text{const.} \quad (20)$$

This condition then simply reads as $2(d_m - 3) + 3/2 \approx 0$ or $d_m \approx 2.25$, which is reasonably close to the observed mass dimension.

As we have shown above, the measured correlation of scaling coefficient u'_0 with the coarse-grained mass surface density of MCs Σ_ℓ is consistent with a purely turbulent nature of their hierarchical structure. The origin of this correlation is rooted in highly compressible nature of the turbulence that implies density dependence of the l.h.s. of equation (14). Let us rewrite equation (15) for the first-order SF of the density-weighted velocity: $\langle |\delta v_\ell| \rangle \sim \langle \epsilon_\ell^{1/3} \rangle \ell^{1/3}$. Due to intermittency, the mean cubic root of the dissipation rate is weakly scale-dependent, $\langle \epsilon_\ell^{1/3} \rangle \propto \ell^{\tau_{1/3}}$, and thus $\langle |\delta v_\ell| \rangle \propto \ell^{\xi_1}$, where $\xi_1 = 1/3 + \tau_{1/3}$ and $\tau_{1/3}$ is the intermittency correction for the dissipation rate. Using dimensional arguments, one can write the scaling coefficient in the Heyer et al. (2009) relation as

$$\delta u_\ell \ell^{-1/2} \propto \rho_\ell^{-1/3} \ell^{-1/6+\tau_{1/3}} \propto \Sigma_\ell^{-1/3} \ell^{1/6+\tau_{1/3}}. \quad (21)$$

Since, as we have shown above, $\Sigma_\ell \propto \ell^{1/3}$, one gets

$$\delta u_\ell \ell^{-1/2} \propto \Sigma_\ell^{1/6+3\tau_{1/3}}. \quad (22)$$

Numerical experiments give $\tau_{1/3} \approx 0.055$ for the density-weighted dissipation rate (Pan, Padoan & Kritsuk 2009). This value implies $\delta u_\ell \ell^{-1/2} \propto \Sigma_\ell^{0.33}$ consistent with the Heyer et al. (2009) data.

To summarize, we have shown that none of the three Larson laws is fundamental, but if one of them is known the other two can be obtained from a single fundamental relation (14) that quantifies the energy transfer rate in compressible turbulence.

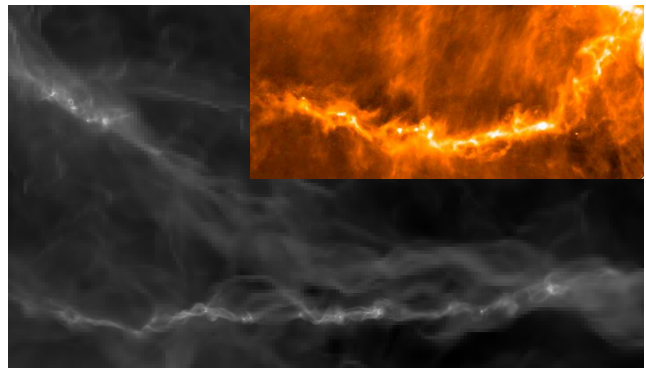


Figure 8. The morphology and size scale of self-gravitating filaments that form in a high dynamic range AMR simulation is similar to that revealed by recent observations. The grey-scale image shows a snapshot of the projected density distribution in a sub-volume of the $(5 \text{ pc})^3$ simulation domain from the self-gravitating model HD3. The image that shows a region of $\sim 3 \text{ pc}$ across was generated using the density field with an effective linear resolution of 8192, while the actual resolution of the simulation was 5×10^5 . The colour inset shows *Herschel* SPIRE 250 μm image of the B211/B213 filament in the Taurus MC (Palmeirim et al. 2012), obtained as part of the *Herschel* Gould Belt survey (André et al. 2010).

6 GRAVITY AND THE BREAKDOWN OF SELF-SIMILARITY

So far, we have limited the discussion of Larson’s relations to scales above the sonic scale. Theoretically, the linewidth–size scaling index is expected to approach $\zeta_1 \approx 1/3$ at $\ell \lesssim \ell_s$ in MC substructures not affected by self-gravity (see Section 2 and Kritsuk et al. 2007a). Falgarone, Pety & Hily-Blant (2009) explored the linewidth–size relation using a large sample of ^{12}CO structures with $\ell \in [10^{-3}, 10^2] \text{ pc}$. These data approximately follow a power law $\delta u_\ell \propto \ell^{1/2}$ for $\ell \gtrsim 1 \text{ pc}$. Although the scatter substantially increases below 1 pc, a slope of 1/3 ‘is not inconsistent with the data’. ^{12}CO and ^{13}CO observations of translucent clouds indicate that small-scale structures down to a few hundred astronomical units are possibly intrinsically linked to the formation process of MCs (Falgarone et al. 1998; Heithausen 2004).

The observed mass–size scaling index, $d_m \approx 2.36$, is expected to remain constant for non-self-gravitating structures down to $\ell_\eta \sim 30\eta$, which is about a few hundred astronomical units, assuming the Kolmogorov scale $\eta \sim 10^{14} \text{ cm}$ (Kritsuk et al. 2011c). This trend is traced down to $\sim 0.01 \text{ pc}$ with the recent *Herschel* detection of ~ 300 unbound starless cores in the Polaris Flare region (André et al. 2010). For scales below $\ell_\eta \sim 200 \text{ au}$, in the turbulence dissipation range, numerical experiments predict convergence to $d_m \approx 2$, as the highest density peaks are located in essentially two-dimensional shock-compressed layers, see Fig. 5.

In star-forming clouds, the presence of strongly self-gravitating clumps of high mass surface density breaks self-similarity imposed by the turbulence. One observational signature of gravity on small scales is the build-up of a high-end power-law tail in the column density PDF. The tail is observationally associated with projected filamentary structures harbouring prestellar cores and young stellar objects (Kainulainen et al. 2009; André et al. 2011).

Fig. 8 illustrates morphological similarity of the B211/B213 filament in the Taurus MC, as imaged by *Herschel* SPIRE at 250 μm , and projected density distribution in a snapshot from the HD3 simulation we discussed in Section 3.2. In these high-resolution images, the knotty fragmented structure of dense cores sitting in the filament and interconnected by a network of thin bow-like fibres forms a distinct pattern. These structures could not have formed as a result of monolithic collapse of gravitationally unstable uniform cylinder. Supersonic turbulence shapes them by creating non-equilibrium initial conditions for local collapses (Schmidt, et al. 2013). Unlike observations, the simulation gives direct access to three-dimensional structure underlying what is seen as a filament in projection. Such projected filamentary structures often include chance overlaps of physically disjoint segments of an intricate fragmented mass distribution created by the turbulence, see Section 4.

A more quantitative approach to comparing observations and numerical simulations of star-forming clouds deals with the column density PDFs. Numerical experiments show that the power index p of the high-density tail of the PDF [$dS(\Sigma) \propto d(\Sigma^p)$, where $p = -2/(n-1)$] is determined by the density profile [$\rho(r) \propto r^{-n}$] of a stable attractive self-similar spherical collapse solution appropriate to specific conditions in a turbulent cloud (Kritsuk et al. 2011b). For model HD3 that includes self-gravity, we obtained $p \simeq -2.5$ and $n \simeq 1.8$ in agreement with theoretical predictions. This implies $d_m = 3 - n \simeq 1.2$ for the mass–size relation on scales $\lesssim 0.1$ pc. Mapping of the actively star-forming Aquila field with *Herschel* gave $p = -2.6 \pm 0.1$ and $d_m = 1.13 \pm 0.07$ for a sample of 541 starless cores with size $\ell \in [0.01, 0.1]$ pc (Könyves et al. 2010; André et al. 2011; Schneider et al. 2013). Using the above formalism, we can predict $d_m = 3 - n = 2 + 2/p \simeq 1.23$, in reasonable agreement with the direct measurement, given a systematic error in p due to the variation of opacity with density (Schneider et al. 2013).

Overall, the expected mass dimension at scales where self-gravity becomes dominant should fall between $d_m = 1$ [Larson-Penston (1969) isothermal collapse solution with $n = 2$] and $d_m = 9/7 \simeq 1.29$ [Penston (1969) pressure-free collapse solution with $n = 12/7$; for more detail see Kritsuk et al. (2011b)].

The characteristic scale where gravity takes control over from turbulence can be predicted using the linewidth–size and mass–size relations discussed in previous sections. Indeed, in a turbulent isothermal gas, the coarse-grained Jeans mass is a function of scale ℓ :

$$m_\ell^J \propto \sigma_\ell^3 \rho_\ell^{-1/2} \propto \begin{cases} \rho_\ell^{-1/2} \propto \ell^{(3-d_m)/2} \propto \ell^{0.32}, & \ell \lesssim \ell_s \\ \delta v_\ell^3 \rho_\ell^{-3/2} \propto \ell^{1+3(3-d_m)/2} \propto \ell^{1.96}, & \ell > \ell_s, \end{cases}$$

where $\sigma_\ell^2 \equiv \delta u_\ell^2 + c_s^2$ (Chandrasekhar 1951) and we assumed that $\sigma_\ell^2 \approx c_s^2$ at $\ell \lesssim \ell_s$, while $\sigma_\ell^2 \approx \delta u_\ell^2$ at $\ell \gtrsim \ell_s$. The dimensionless stability parameter, $\mu_\ell \equiv m_\ell/m_\ell^J$, shows a strong break in slope at the sonic scale:

$$\mu_\ell \propto \begin{cases} \ell^{3(d_m-1)/2} \propto \ell^{2.04} & \text{if } \ell \lesssim \ell_s \\ \ell^{(5d_m-11)/2} \propto \ell^{0.4} & \text{if } \ell > \ell_s, \end{cases}$$

and a rather mild growth above ℓ_s . Since both μ_ℓ and the free-fall time,

$$t_\ell^{\text{ff}} \equiv [3\pi/(32G\rho_\ell)]^{1/2} \propto \ell^{(3-d_m)/2} \propto \ell^{0.32}, \quad (23)$$

correlate positively with ℓ , a *bottom-up* non-linear development of Jeans instability is most likely at $\ell \gtrsim \ell_J$, where $\mu_{\ell_J} = 1$. This assessment is supported by simulations discussed in Section 3.2, which successfully reproduce observed morphology of filaments (Fig. 8) and density distributions. Note that both μ_ℓ and t_ℓ^{ff} grow approximately linearly (i.e. relatively weakly) with Σ_ℓ at $\ell > \ell_s$, while below the sonic scale $\mu_\ell \propto \Sigma_\ell^7$. This means that the instability, when present, shuts off very quickly below ℓ_s , i.e. $\ell_J \sim \ell_s$. The formation of prestellar cores would be possible only in sufficiently over-dense regions on scales around $\ell_s \sim 0.1$ pc. The sonic scale, thus, sets the characteristic mass of the core mass function, m_{ℓ_s} , and the threshold mass surface density for star formation, Σ_{ℓ_s} (cf. Krumholz & McKee 2005; André et al. 2010; Padoan & Nordlund 2011).³

As supersonic turbulence creates seeds for self-gravitating cores, one can use scaling relations derived above to predict the core mass function (CMF). The geometry of turbulence controls the number of overdense clumps as a function of their size, $N(\ell) \propto \ell^{-d_m}$. The differential size distribution, $dN(\ell) \propto \ell^{-(1+d_m)} d\ell$, together with the marginal stability condition⁴ determine the high-mass end of the CMF. Indeed, for $m_\ell = m_\ell^J \propto \ell^{1+3(3-d_m)/2}$, we obtain a power-law distribution:

$$dN(m) \propto m^{-\alpha} dm, \quad (24)$$

where

$$\alpha = (11 - d_m)/(11 - 3d_m) \simeq (7 + 3\zeta_1)/(9\zeta_1 - 1) \quad (25)$$

is reasonably close to Salpeter’s index of 2.35 (cf. Padoan & Nordlund 2002). For instance, if $\zeta_1 = \{0.5, 0.56\}$, we get $\alpha = \{2.43, 2.15\}$, while $d_m = \{2.36, 2.5\}$ gives $\alpha = \{2.20, 2.43\}$.

7 CONCLUSIONS AND FINAL REMARKS

We have shown that, with current observational data for large samples of Galactic MCs, Larson’s relations on scales 0.1 – 50 pc can be consistently interpreted as an empirical signature of supersonic turbulence fed by the large-scale kinetic energy injection. Our interpretation is based on a theory of highly compressible turbulence and supported by high-resolution numerical simulations. Independently, this picture is corroborated by often elongated shape of GMCs and their internal filamentary or sheet-like structures (e.g. Bally et al. 1989; Blitz 1993; Molinari et al. 2010).

Our simulations do not rule out the importance of gravitational effects on scales comparable to the disc scale-height, where the dynamics become substantially more

³ Our arguments here should be taken with a grain of salt as the Jeans stability criterion we relied on is based on the turbulent support concept (Chandrasekhar 1951; Bonazzola et al. 1992) originally developed for scales above the turbulent energy injection scale, see Section 1. In star-forming MCs, the injection scale is believed to be much larger than the sonic length. This illustrates the limits of phenomenological approach based on dimensional analysis.

⁴ $\mu_\ell = 1$ is a prerequisite for the formation of bound cores from turbulent clumps based on the Chandrasekhar (1951) phenomenology.

complex. Large-scale gravitational instabilities in galactic discs including both stellar and gaseous components (e.g. Hoffmann & Romeo 2012) can power a three-dimensional direct energy cascade towards smaller scales and a quasi-two-dimensional inverse energy cascade to larger scales (Elmegreen et al. 2001, 2003a,b; Bounaud et al. 2010; Renaud et al. 2013). These instabilities can play a significant role in accumulating the largest and most massive GMCs that appear gravitationally bound in observations (e.g. Heyer et al. 2001; Ballesteros-Paredes et al. 2007; McKee et al. 2010; Hennebelle & Falgarone 2012).⁵ Our models implicitly include the combined effects of sheared disc instabilities as well as the star formation feedback through the external large-scale energy injection that powers the turbulence. This simplified treatment does not account for the competition between the large-scale gravity and the feedback, which keeps the ISM in a self-regulated statistical steady state with GMCs continuously forming, dispersing, and re-forming (Hopkins et al. 2012). The resulting net energy injection rate, however, enters as an input parameter in our models and can be estimated theoretically (Faucher-Giguère et al. 2013) and constrained observationally (see Section 3.3).

On small scales, in low-density translucent clouds, self-similarity of turbulence can potentially be preserved down to $\sim 10^{-3}$ pc, where dissipation becomes important. In contrast, in overdense regions, the formation of prestellar cores breaks the turbulence-induced scaling and self-gravity assumes control over the slope of the mass-size relation. The transition from turbulence- to gravity-dominated regime in this case occurs close the sonic scale $\ell_s \sim 0.1$ pc, where structures turn gravitationally unstable first, leading to the formation of prestellar cores.

While some will reason that the virial interpretation does not necessarily imply clouds are virialized or even bound and call the acceptance of a turbulent interpretation of Larson's laws an extreme, others argue that this step solves a number of outstanding problems: it (i) explains inefficient star formation; (ii) explains the origin and inter-relationship of Larson's laws; (iii) naturally includes the relationship between GMCs and larger-scale ISM; and finally (iv) it provides a self-consistent framework for cloud and star formation modelling – all based on the same set of observational cloud properties. Moreover, the turbulent interpretation removes other questions previously considered crucial in the isolated cloud framework, e.g. whether MC turbulence is driven or decaying, as clouds are born turbulent.

Our approach is based on a theoretical description of turbulent cascade and the results are valid in a statistical sense. This means that the scaling relations we discuss hold for sufficiently large ensemble averages. Relations obtained for individual MCs and elements of their internal substructure, as well as relations based on different tracers, can show substantial statistical variations around the mean. The scaling exponents we discuss or derive are usually accurate within $\approx (5 - 10)$ per cent, while scaling coefficients bear substantial systematic errors. Homogeneous multiscale sampling of a large number of MCs and their substructure (in-

cluding both kinematics and column density mapping) with CCAT, *SOFIA*, *JWST* and ALMA will help to detail the emerging picture discussed above.

ACKNOWLEDGEMENTS

We thank Philippe André for providing the scaling exponents from *Herschel* mapping of the Aquila field and for sharing an image of the B211/213 Taurus filament prior to publication. We are grateful to Sergey Ustyugov for sharing data from the multiphase simulation we used to generate Figs 3 and 4. We appreciate Richard Larson's comments on an early version of the manuscript, which helped to improve the quality of presentation. This research was supported in part by NSF grants AST-0808184, AST-0908740, AST-1109570, and by XRAC allocation MCA07S014. Simulations and analysis were performed on the DataStar, Trestles, and Triton systems at the San Diego Supercomputer Center, UCSD, and on the Kraken and Nautilus systems at the National Institute for Computational Science, ORNL.

REFERENCES

- Aluie H., 2011, *Phys. Rev. Lett.*, 106, 174502
 Aluie H., Li S., & Li H., 2012, *ApJL*, 751, L29
 Aluie H., 2013, *Physica D*, 247, 54
 André P., Men'shchikov A., Könyves V., Arzoumanian D., 2011, in J. Alves, B. G. Elmegreen, J. M. Girart, V. Trimble, eds, *Proc. IAU Symp. 270, Computational Star Formation*. Cambridge Univ. Press, Cambridge (UK), p. 255
 André P., Men'shchikov A., Bontemps S., et al., 2010, *A&A*, 518, L102
 Ballesteros-Paredes J., Mac Low M.-M., 2002, *ApJ*, 570, 734
 Ballesteros-Paredes J., 2006, *MNRAS*, 372, 443
 Ballesteros-Paredes J., Klessen R. S., Mac Low M.-M., Vazquez-Semadeni E., 2007, *Protostars and Planets V*, 63
 Ballesteros-Paredes J., Hartmann L. W., Vázquez-Semadeni E., Heitsch F., Zamora-Avilés M. A., 2011, *MNRAS*, 411, 65
 Ballesteros-Paredes J., Vazquez-Semadeni E., Gazol A., Hartmann L. W., Heitsch F., Colin P., 2011, *MNRAS*, 416, 1436
 Ballesteros-Paredes J., D'Alessio P., Hartmann L., 2012, *MNRAS*, 427, 2562
 Bally J., Stark A. A., Wilson R. W., Langer W. D., 1989, in *Lecture Notes in Physics*, Vol. 331, *The Physics and Chemistry of Interstellar Molecular Clouds – mm and Sub-mm Observations in Astrophysics*. Springer-Verlag, Berlin, p. 81
 Banerjee S., & Galtier S. 2013, *Phys. Rev. E*, 87, 013019
 Bertoldi F., McKee C. F., 1992, *ApJ*, 395, 140
 Biglari H., Diamond P. H., 1988, *Phys. Rev. Lett.*, 61, 1716
 Blitz L., 1987, in G. E. Morfill, M. Scholer, eds, *Proc. NATO ASIC, Vol. 210, Physical Processes in Interstellar Clouds*. D. Reidel Publishing Co., Dordrecht, p. 35
 Blitz L., 1993, in *Protostars and Planets III*. University of Arizona Press, p. 125

⁵ The dual cascade picture, however, narrows the applicability of virial relation (2) even further.

- Bolatto A. D., Leroy A. K., Rosolowsky E., Walter F., Blitz L., 2008, *ApJ*, 686, 948
- Boldyrev S., 2002, *ApJ*, 569, 841
- Bonazzola S., Heyvaerts J., Falgarone E., Perault M., Puget J. L., 1987, *A&A*, 172, 293
- Bonazzola S., Perault M., Puget J. L., et al., 1992, *J. Fluid Mech.*, 245, 1
- Bournaud F., Elmegreen B. G., Teyssier R., Block D. L., Puerari I., 2010, *MNRAS*, 409, 1088
- Brunt C. M., 2003a, *ApJ*, 583, 280
- Brunt C. M., 2003b, *ApJ*, 584, 293
- Chandrasekhar S., 1951, *Roy. Soc. London Proc. Ser. A*, 210, 26
- Chieze J. P., 1987, *A&A*, 171, 225
- Colella P., & Woodward P. R., 1984, *J. Comp. Phys.*, 54, 174
- Collins D. C., Kritsuk A. G., Padoan P., Li H., Xu H., Ustyugov S. D., Norman M. L. 2012, *ApJ*, 750, 13
- de Avillez M. A., Breitschwerdt D., 2007, *ApJ*, 665, L35
- Dib S., Kim J., Vázquez-Semadeni E., Burkert A., Shadmehri M., 2007, *ApJ*, 661, 262
- Dobbs C. L., Burkert A., Pringle J. E., 2011, *MNRAS*, 413, 2935
- Dubrulle, B. 1994, *Phys. Rev. Lett.*, 73, 959
- Elmegreen B. G., Falgarone E., 1996, *ApJ*, 471, 816
- Elmegreen B. G., Kim S., & Staveley-Smith L., 2001, *ApJ*, 548, 749
- Elmegreen B. G., Elmegreen D. M., & Leitner S. N., 2003, *ApJ*, 590, 271
- Elmegreen B. G., Leitner S. N., Elmegreen D. M., & Cuilandre J.-C., 2003, *ApJ*, 593, 333
- Elmegreen B. G., Scalo J., 2004, *ARA&A*, 42, 211
- Falgarone E., Phillips T. G., 1991, *Fragmentation of Molecular Clouds and Star Formation*, 147, 119
- Falgarone E., Lis D. C., Phillips T. G., et al., 1994, *ApJ*, 436, 728
- Falgarone E., Panis J.-F., Heithausen A., et al., 1998, *A&A*, 331, 669
- Falgarone E., Pety J., Hily-Blant P., 2009, *A&A*, 507, 355
- Falkovich G., Fouxon I., Oz Y., 2010, *J. Fluid Mech.*, 644, 465
- Faucher-Giguère C.-A., Quataert E., & Hopkins P. F., 2013, *MNRAS*, 433, 1970
- Federrath C., Klessen R. S., Schmidt W., 2009, *ApJ*, 692, 364
- Federrath C., Roman-Duval J., Klessen R. S., Schmidt W., Mac Low M.-M., 2010, *A&A*, 512, A81
- Federrath C., 2013, *MNRAS*, in press, doi:10.1093/mnras/stt1644
- Field G. B., 1965, *ApJ*, 142, 531
- Fleck R. C., Jr., 1983, *ApJ*, 272, L45
- Fleck R. C., Jr., 1996, *ApJ*, 458, 739
- Frisch U., 1995, *Turbulence. The legacy of A. N. Kolmogorov*. Cambridge Univ. Press, Cambridge (UK)
- Galtier S., Banerjee S., 2011, *Phys. Rev. Lett.*, 107, 134501
- Gent F. A., Shukurov A., Fletcher A., Sarson G. R., Mantere M. J., 2013, *MNRAS*, 432, 1396
- Goodman A. A., Rosolowsky E. W., Borkin M. A., Foster J. B., Halle M., Kauffmann J., Pineda J. E., 2009, *Nat*, 457, 63
- Gotoh T., 2002, *Comput. Phys. Comm.*, 147, 530
- Heiles C., 2001, *ApJ*, 551, L105
- Heiles C., & Crutcher R. 2005, *Cosmic Magnetic Fields*, *Lect. Notes Phys.*, 664, 137
- Heithausen A., 2004, *ApJ*, 606, L13
- Hennebelle P., Chabrier G., 2008, *ApJ*, 684, 395
- Hennebelle P., Chabrier G., 2011, *ApJ*, 743, L29
- Hennebelle P., Falgarone E., 2012, *A&AR*, 20, 55
- Henriksen R. N., Turner B. E., 1984, *ApJ*, 287, 200
- Henriksen R. N., 1991, *ApJ*, 377, 500
- Heyer M. H., Schloerb F. P., 1997, *ApJ*, 475, 173
- Heyer M. H., Carpenter J. M., Snell R. L., 2001, *ApJ*, 551, 852
- Heyer M. H., Brunt C. M., 2004, *ApJ*, 615, L45
- Heyer M., Krawczyk C., Duval J., Jackson J. M., 2009, *ApJ*, 699, 1092
- Hoffmann V., & Romeo A. B., 2012, *MNRAS*, 425, 1511
- Hopkins P. F., Quataert E., & Murray N., 2012, *MNRAS*, 421, 3488
- Hunter J. H., Jr., 1970, *ApJ*, 161, 451
- Ishihara T., Gotoh T., & Kaneda Y., 2009, *Ann. Rev. Fluid Mech.*, 41, 165
- Jenkins E. B., Tripp T. M., 2011, *ApJ*, 734, 65
- Joung M. K. R., Mac Low M.-M., 2006, *ApJ*, 653, 1266
- Kainulainen J., Beuther H., Henning T., Plume R., 2009, *A&A*, 508, L35
- Kaneda Y., Ishihara T., Yokokawa M., Itakura K., & Uno A., 2003, *Phys. Fluids*, 15, L21
- Kegel W. H., 1989, *A&A*, 225, 517
- Klessen R. S., 2000, *ApJ*, 535, 869
- Koda J., Sawada T., Hasegawa T., Scoville N. Z., 2006, *ApJ*, 638, 191
- Kolmogorov A. N., 1941a, *Dokl. Akad. Nauk SSSR*, 30, 299
- Kolmogorov A. N., 1941b, *Dokl. Akad. Nauk SSSR*, 32, 19
- Kolmogorov A. N., 1962, *J. Fluid Mech.*, 13, 82
- Könyves V., André P., Men'shchikov A., et al., 2010, *A&A*, 518, L106
- Kowal G., Lazarian A., 2007, *ApJ*, 666, L69
- Kritsuk A. G., Norman M. L., 2002, *ApJ*, 569, L127
- Kritsuk A. G., Norman M. L., 2004, *ApJ*, 601, L55
- Kritsuk A. G., Wagner R., Norman M. L., Padoan P., 2006a, in N. V. Pogorelov, G. P. Zank, eds, *ASP Conf. Ser.*, Vol. 359, *Numerical Modeling of Space Plasma Flows*. Astron. Soc. Pac., San Francisco, p. 84
- Kritsuk A. G., Norman M. L., Padoan P., 2006b, *ApJ*, 638, L25
- Kritsuk A. G., Norman M. L., Padoan P., Wagner R., 2007a, *ApJ*, 665, 416
- Kritsuk A. G., Padoan P., Wagner R., Norman M. L., 2007b, in D. Shaikh, G. P. Zank, eds, *AIP Conf. Proc.*, Vol. 932, *Turbulence and Nonlinear Processes in Astrophysical Plasmas*. New York, p. 393
- Kritsuk A. G., Ustyugov S. D., Norman M. L., Padoan P., 2009, in N. V. Pogorelov, E. Audit, P. Colella, G. Zank, eds, *ASP Conf. Ser.*, Vol. 406, *Numerical Modeling of Space Plasma Flows*. Astron. Soc. Pac., San Francisco, p. 15
- Kritsuk A. G., Ustyugov S. D., Norman M. L., Padoan P., 2010, in N. V. Pogorelov, E. Audit, G. Zank, eds, *ASP Conf. Ser.*, Vol. 429, *Numerical Modeling of Space Plasma Flows*. Astron. Soc. Pac., San Francisco, p. 15
- Kritsuk A. G., Ustyugov S. D., Norman M. L., 2011a, in J. Alves, B. G. Elmegreen, J. M. Girart, V. Trimble, eds, *Proc. IAU Symp.* 270, *Computational Star Formation*.

- Cambridge Univ. Press, Cambridge (UK), p. 179
- Kritsuk A. G., Norman M. L., Wagner R., 2011b, *ApJ*, 727, L20
- Kritsuk A. G., Nordlund Å., Collins D., et al., 2011c, *ApJ*, 737, 13
- Kritsuk A. G., Wagner R., & Norman M. L., 2013, *J. Fluid Mech.*, 729, R1
- Krumholz M. R., McKee C. F., 2005, *ApJ*, 630, 250
- Landau L. D., Lifshitz E. M., 1987, *Fluid Mechanics*, Pergamon Press, Oxford
- Larson R. B., 1969, *MNRAS*, 145, 271
- Larson R. B., 1981, *MNRAS*, 194, 809
- Lequeux J., 2005, *The Interstellar Medium*, Astronomy and Astrophysics Library. Springer-Verlag, Berlin
- Lombardi M., Alves J., Lada C. J., 2010, *A&A*, 519, L7
- Mac Low M.-M., 1999, *ApJ*, 524, 169
- Mac Low M.-M., Klessen R. S., 2004, *Rev. Mod. Phys.*, 76, 125
- McKee C. F., Li P. S., Klein R. I., 2010, *ApJ*, 720, 1612
- McKee C. F., Zweibel E. G., 1992, *ApJ*, 399, 551
- McKee C. F., Ostriker E. C., 2007, *ARA&A*, 45, 565
- Miesch M. S., Bally J., 1994, *ApJ*, 429, 645
- Molinari S., Swinyard B., Bally J., et al., 2010, *A&A*, 518, L100
- Moyal J. E., 1952, *Proceedings of the Cambridge Philosophical Society*, 48, 329
- Myers P. C., 1983, *ApJ*, 270, 105
- Nordlund Å., Padoan P., 2003, in E. Falgarone, T. Passot., eds, *Turbulence and Magnetic Fields in Astrophysics*, Lecture Notes in Physics, Vol. 614, p. 271
- Ostriker E. C., Stone J. M., Gammie C. F., 2001, *ApJ*, 546, 980
- Padoan P., Nordlund Å., 2011, *ApJ*, 730, 40
- Padoan P., Nordlund Å., Kritsuk A. G., Norman M. L., Li P. S., 2007, *ApJ*, 661, 972
- Padoan P., Cambrésy L., Juvela M., Kritsuk A., Langer W. D., Norman M. L., 2006, *ApJ*, 649, 807
- Padoan P., Kritsuk A., Norman M. L., Nordlund Å., 2005, *ApJ*, 622, L61
- Padoan P., Nordlund Å., 2002, *ApJ*, 576, 870
- Palmeirim P. M., André Ph., Kirk J., et al. 2013, *A&A*, 550, A38
- Pan L., Padoan P., Kritsuk A. G., 2009, *Phys. Rev. Lett.*, 102, 034501
- Passot T., Pouquet A., Woodward P., 1988, *A&A*, 197, 228
- Penston M. V., 1969, *MNRAS*, 144, 425
- Porter D. H., Pouquet A., Woodward P. R., 1994, *Physics of Fluids*, 6, 2133
- Price D. J., & Federrath C. 2010, *MNRAS*, 406, 1659
- Renaud F., Bournaud F., Emsellem E., et al., 2013, *MNRAS*, accepted, arXiv:1307.5639
- Richardson L. F., 1922, *Weather Prediction by Numerical Process*, Cambridge University Press
- Robertson B., Goldreich P., 2012, *ApJ*, 750, L31
- Roman-Duval J., Federrath C., Brunt C., et al., 2011, *ApJ*, 740, 120
- Roman-Duval J., Jackson J. M., Heyer M., Rathborne J., Simon R., 2010, *ApJ*, 723, 492
- Scalo J., 1990, in *Physical Processes in Fragmentation and Star Formation*, Kluwer Acad. Publ., Dordrecht, p. 151
- Schmidt W., Federrath C., 2011, *A&A*, 528, A106
- Schmidt W., Federrath C., Hupp M., Kern S., Niemeyer J. C., 2009, *A&A*, 494, 127
- Schmidt W., Federrath C., Klessen R., 2008, *Phys. Rev. Lett.*, 101, 194505
- Schmidt W., Collins D. C., Kritsuk A. G., 2013, *MNRAS*, 431, 3196
- Schneider N., Brooks K., 2004, *Proc. Astron. Soc. Australia*, 21, 290
- Schneider N., André P., Könyves V., et al., 2013, *ApJL*, 766, L17
- Schwarz C., Beetz C., Dreher J., Grauer R., 2010, *Physics Letters A*, 374, 1039
- She Z.-S., Leveque E., 1994, *Phys. Rev. Lett.*, 72, 336
- Shetty R., Collins D. C., Kauffmann J., et al. 2010, *ApJ*, 712, 1049
- Solomon P. M., Rivolo A. R., Barrett J., Yahil A., 1987, *ApJ*, 319, 730 (SRBY87)
- The Enzo Collaboration: Bryan G. L., Norman M. L., et al., 2013, arXiv:1307.2265
- Truelove J. K., Klein R. I., McKee C. F., et al., 1997, *ApJL*, 489, L179
- Ungerechts H., Thaddeus P., 1987, *ApJS*, 63, 645
- Ustyugov S. D., Popov M. V., Kritsuk A. G., & Norman M. L., 2009, *J. Comp. Phys.*, 228, 7614
- von Hoerner S., 1951, *Zeitschrift für Astrophysik*, 30, 17
- von Weizsäcker C. F., 1951, *ApJ*, 114, 165
- Wagner R., Falkovich G., Kritsuk A. G., Norman M. L., 2012, *J. Fluid Mech.*, 713, 482
- White R. E., 1977, *ApJ*, 211, 744
- Wolfire M. G., Hollenbach D., McKee C. F., Tielens A. G. G. M., Bakes E. L. O., 1995, *ApJ*, 443, 152
- Zinnecker H., 1984, *MNRAS*, 210, 43
- Zrake J., MacFadyen A. I., 2012, *ApJ*, 744, 32

This paper has been typeset from a \TeX / \LaTeX file prepared by the author.